On the Response of 7000-Series Aluminum Alloys to Hot Stamping

by

Kaab Omer

A thesis

presented to the University of Waterloo

in fulfilment of the

thesis requirement for the degree of

Doctor of Philosophy

in

Mechanical and Mechatronics Engineering

Waterloo, Ontario, Canada, 2019

Examining Committee Membership

The following served on the Examining Committee for this thesis. The decision of the Examining Committee is by majority vote.

Supervisors	Michael Worswick, PhD Professor, University of Waterloo
	Shahrzad Esmaeili, PhD Professor, University of Waterloo
External Examiner	Farhang Pourboghrat, PhD Professor, Ohio State University
Internal Examiner	Clifford Butcher, PhD Assistant Professor, University of Waterloo
Internal Examiner	Adrian Gerlich, PhD Associate Professor, University of Waterloo
Internal-External Examiner	Sriram Narasimhan, PhD Professor, University of Waterloo

Author's Declaration

This thesis consists of material all of which I authored or co-authored (see Statement of Contributions included in the thesis).

This is a true copy of the thesis, including any required final revisions, as accepted by my examiners.

I understand that my thesis may be made electronically available to the public.

Statement of Contributions

The following co-authors have contributed to the current work:

Professor Michael Worswick and Professor Shahrzad Esmaeili supervised this work.

Professor Clifford Butcher advised on the constitutive modelling, yield surface calibration and the heat transfer aspects of this work.

Atekeh Abolhasani performed some of the tensile tests shown in Appendix D, and all of the calorimetry work in Appendix D. She also provided the kinetic hardening parameters, which were used in the work hardening rate model.

The balance of the research is my own work.

Abstract

Hot stamping, or die quenching (DQ), of 7000-series aluminum alloys is a metal forming process in which a blank is heated (solutionized) and then quenched and formed in cold tooling. The formed part is then subjected to an artificial aging treatment to reach a targeted final strength (temper). The work presented herein addresses several aspects of the die quenching process chain for two 7000-series aluminum sheet alloys, AA7075 and a developmental alloy referred to as AA7xxx. The thesis addresses: (i) identification of forming process and artificial aging parameters needed to achieve high strength structural properties within an automotive die quenching paradigm; (ii) characterization of high temperature constitutive and heat transfer properties required to accurately simulate the die quenching process; and (iii) development of a model of the work hardening response of die quenched AA7075 as a function of the extent of artificial aging.

The effect of the solutionizing duration, the transfer time between the furnace and die, and the in-die quench rate on the subsequent aging response were examined for both alloys. Experiments revealed that both alloys require a solutionizing time of 8 min at 470 °C. For AA7075, a transfer time of up to 6 s (furnace to die) was deemed to be acceptable since this time duration does not appear to result in premature precipitation. For AA7xxx, a transfer time of up to 15 s is acceptable. AA7075 required a minimum quench rate of 56 °C/s, whereas AA7xxx requires only 27 °C/s. Variations in aging treatments following die quenching were also considered in order to obtain desirable yield and ultimate tensile strength properties while accounting for the paint bake cycle (PBC) and its effect on artificial aging response. It was determined that AA7075 could achieve strength properties similar to those a T6 temper if it was aged for 8h at 121 °C followed

by a PBC (30 min at 177 °C). AA7xxx could achieve T6-like properties if aged for 3h at 100 °C followed by a PBC and T76-like properties if aged for 4h at 100 °C, followed by a PBC.

A detailed characterization of the constitutive behaviour and heat transfer characteristics of these alloys under DQ conditions was performed. Of particular note, this characterization was performed at elevated temperatures while the material was in a solutionized condition. The acquired properties consisted of: (i) the temperature and strain rate dependent stress-strain properties; (ii) the yield surface, and (iii) the heat transfer coefficient (HTC) of both alloys. The stress-strain properties were obtained by subjecting tensile specimens to a temperature-time cycle resembling the DQ process. A novel technique was devised in which the cross-sectional area of the tensile specimens were measured using stereoscopic digital image correlation (DIC) technique. A Barlat Yld2000 yield surface was calibrated using anisotropic properties obtained from shear and tensile tests. The HTC was obtained as a function of contact pressure by performing a series of instrumented quenching experiments in which the temperatures of the blank and die were measured as a function of time. These temperature-time curves were processed using Fourier's law and Newton's cooling law to calculate HTC.

The acquired elevated temperature constitutive properties and heat transfer coefficients were input to a finite element model of die quenched deep drawn cups. The load-displacement and earring profile results from the experiments were shown to match well with the predicted results from the model.

The final step in the DQ process chain was also considered in terms of the final or in-service mechanical properties of die quenched and artificially aged components. A micro-mechanics based model was developed to predict the stress-strain response and work hardening rate of

AA7075 as a function of the aging treatment applied. The micromechanics model accounts for precipitate-dislocation interaction during deformation following aging and was validated for a range of multi-step aging treatments. Tensile tests were performed considering tempers ranging from as-quenched up to the peak aged condition, and the model was shown to accurately predict flow stress over the entire range of aging treatments considered.

Acknowledgements

I would like to thank my supervisor, Professor Michael Worswick, for allowing me to work on this project and for his guidance and mentorship throughout my PhD. His emphasis on proper testing technique, good writing style and presentation of results have been invaluable. In addition to his direct mentorship, I have taken many lessons from him indirectly just by observing his ability to juggle between several tasks. I am truly grateful that I had the opportunity to work under his supervision over the last few years. I would also like to thank my co-supervisor, Professor Shahrzad Esmaeili, for her guidance on the microstructural aspect of my work and for her patient explanations on various topics. Without her, large sections of this thesis would not have been possible.

Professor Clifford Butcher helped me tremendously with the yield surface fitting, and with the area reduction method, as well as providing general guidance throughout this work, and I am very grateful for it. A shout-out goes to another PhD student, Atekeh Abolhasani, without whom my work hardening rate model would not have been possible. Other people without whom this thesis would not have been possible are Eckhard Budziarek, Laurie Wilfong, Ryan George, Tom Gawel, Jeff Wemp, the guys at EMS, Andy Barber and Neil Griffett.

I will always remember Samuel Kim and Nikky Pathak for our coffee walks and movie nights. Ania Polak made my experience in EC4 very memorable. Credit goes to Bartek Pilarczyk for expanding my cultural horizons. Chris Kohar and I have spent many long nights together entertaining each other. Pedram Samadian has taught me many conceptual things.Though I pretend to be upset, I am always happy by the distractions of Steven Lee, Nick Aydemir and Edward Gutierrez. Thank you guys for making my grad studies experience so colourful!

I would like to thank Honda R&D Americas Inc., Arconic Ground Transportation Group, Promatek Research Centre, the Natural Sciences and Engineering Research Council (NSERC), the Canada Foundation for Innovation, the Ontario Research Fund, the Ontario Centres of Excellence, the Ontario Advanced Manufacturing Consortium, and the Canada Research Chairs Secretariat for financial support of this research.

List of Figures and Tables

1. Introduction

The 7000-series aluminum alloys are heat treatable and contain Zinc as their primary alloying element. These alloys are used extensively in the aerospace sector; however, more recently, the automotive industry has shown increased interest in these alloys for structural applications due to their high strength and excellent light weighting potential. An important challenge in utilizing 7000-series alloys is that they tend to exhibit poor formability at room temperature [1,2].

One approach that can significantly increase the formability of these alloys is hot stamping through a what is referred to as a hot forming or a die quenching (DQ) process. In the DQ process, an aluminum blank is solutionized in a furnace and subsequently quenched and formed in a chilled die set [3,4]. The solutionizing process dissolves the precipitates present in the alloy into the broader Al matrix. The dissolution of precipitates greatly reduces the strength of the alloy at the elevated temperature, but also increases its ductility, thereby increasing formability [2,5]. A characteristic of the DQ process is that the blank undergoes a rapid quench during the forming operation. This rapid quench results in achieving a supersaturated solid solution (SSS) state of the alloy. The as-formed part can then be artificially aged to achieve high strength.

This thesis focuses on three main challenges or focus areas associated with the DQ process:

1. The determination of necessary process parameters for a successful DQ forming and quenching operation.
2. Determination of the material properties and heat transfer coefficients that are necessary to accurately simulate the DQ process.

3. Development of a model to predict the stress-strain properties of die quenched, as-formed components after the application of an artificial aging treatment used to achieve targeted final properties.

This thesis is written in a manuscript-style format, which comprises this synopsis and four journal papers, incorporated as Appendices A-D. This synopsis provides a high-level summary of the thesis outcomes and the integration of the overall results, while the appendices provide more detailed results on each sub-topic.

The remainder of this synopsis will cover the following. Chapter 2 presents a review of the scientific literature relevant to this research (a more detailed literature review is found in each of the individual journal papers in the appendices). Chapter 3 presents the overall research objectives and scope of this work. Chapter 4 provides a synopsis of the results (with more detailed discussion included in Appendices A-D). Chapter 5 provides a discussion of the results and conclusions stemming from this research, while recommendations for future work are given in Chapter 6.

2. Literature Review

2.1. Material Processing Parameters for Die Quenching of 7000-Series Alloys

7000-series aluminum alloys are characterized by the presence of Zinc as their primary alloying element. In general, these alloys have higher strengths then 6000- and 5000-series alloys. A strengthening heat treatment process for aluminum alloys generally starts with a solutionizing phase. For AA7075, the solutionizing temperature is typically around 470 °C [6]. At this temperature, the atoms present in the precipitates dissolve into the Al matrix, and thus the material enters a single phase or solutionized state. The solutionized alloy is then quenched in water, where it enters a supersaturated solid solution (SSS) state [7], and then aged to a desired temper. This entire process is usually performed by the aluminum producer. However, in the DQ process, the first two steps of the process, namely the solutionizing and rapid quenching steps, are combined with a metal forming operation.

One issue that arises from combining the heat treatment and metal forming operations is the minimum time required to achieve a solutionized state in the to-be-formed blank, *i.e.*, the total soak time. Most studies in the literature use a total soak time ranging from 30 minutes to 4 hours [8–12]. From a metal forming production efficiency perspective, however, soak times of 30 minutes to 4 hours are too long. Rokni *et al.* [5] used a soak time of 7 minutes in their experiments. However, they did not provide a rationale for selecting this number in their study.

Another issue that arises from adapting the heat treatment procedure into the DQ process is that of quench rate. Caron *et al.* [13] showed that the heat transfer coefficient (HTC) of a blank tends to be significantly higher when quenched in water, as opposed to while being formed in steel dies. Therefore, the cooling rate during a DQ process will be lower than a cooling rate during a

water quench. The lower quench rate during die quenching is of particular concern in the case of AA7075 due to what is referred to as high "quench sensitivity". A high quench sensitivity indicates that the cooling rate during quenching has a significant effect on the properties of the alloy after quenching. Deschamps *et al.* [14] showed that lower quench rates result in a lower volume fraction of Guinier-Preston (GP) zones in the as-quenched material, which in turn results in fewer nucleation sites for η′ particles to form during subsequent natural aging. Furthermore, the precipitates formed during quenching are located around grain boundaries that will likely increase the chances of stress corrosion cracking in the material [1,15–19].

Robinson *et al.* [12] and Liu *et al.* [20] showed that the chromium present in AA7075 results in large incoherent dispersoids that act as nucleation sites for precipitation hardening during artificial aging. Liu *et al.* [21] similarly showed that the presence of zirconium and Al_3Zr particles decreases the quench sensitivity of AA7085 alloy. During a rapid quench, there is not enough time for precipitates to form around the dispersoids and so more precipitates remain in solution. During a slow quench, more time is available for precipitation to occur at these nucleation sites, resulting in lower dissolved solute availability for subsequent age hardening thermal treatment. Liu *et al.* [22] solutionized AA7055, then quenched it in cold water, boiling water and air. Their tensile results showed a drop of up to 20% in yield and UTS between samples quenched in cold water and those quenched in air. Other studies that have reached similar conclusions on quench rate sensitivity can be found in [23–27].

In DQ operations, the "transfer time" refers to the time elapsed between the moment that the blank is removed from the oven to the time at which forming and die quenching commences. During this time, the blank is subjected to air cooling. Liu *et al.* [20] showed that the critical temperature (*i.e.*, the temperature below which precipitation begins) is 415 °C for AA7075 and

367 °C for AA7085. Other sources have also reported that the critical temperature for AA7075 is in the 410-420 °C range [28,29]. During the DQ process, should the blank temperature dip below these temperatures during the transfer cycle, it would have detrimental effects on the age hardenability of the formed part. Note that the critical temperatures cited in all these studies were obtained based on very slow heat up and cooling times (i.e., almost isothermal conditions).

The transfer in the DQ process, however, is not an isothermal event. You *et al.* [25] showed that a transfer time of up to 20s does not significantly alter the strength and age hardenability of AA7055.

2.2. Constitutive Properties of 7000-Series Alloys

2.2.1. Elevated Temperature Properties

At elevated temperatures, 7000-series aluminum alloys tend to become softer and more sensitive to strain rate than at room temperature. Rajamuthamilselvan and Ramanathan [4] performed tensile tests on AA7075 at temperatures ranging from 350 °C to 500 °C, using strain rates ranging from 0.001 s^{-1} to 1.0 s^{-1}. Rokni *et al.* [5] did similar testing ranging from 450 °C to 580 °C, for the following strain rates: 0.004 s^{-1}, 0.04 s^{-1} and 0.4 s^{-1}. Lee *et al.* [30] obtained stress-strain properties in the range 25 °C to 300 °C. Results from all three studies are shown in Figure 1; however, none of these studies employed any kind of a quenching mechanism. In other words, all of the three aforementioned studies simply heated the AA7075 to the stated temperature, such that the material was not quenched as would be the case during die quenching.

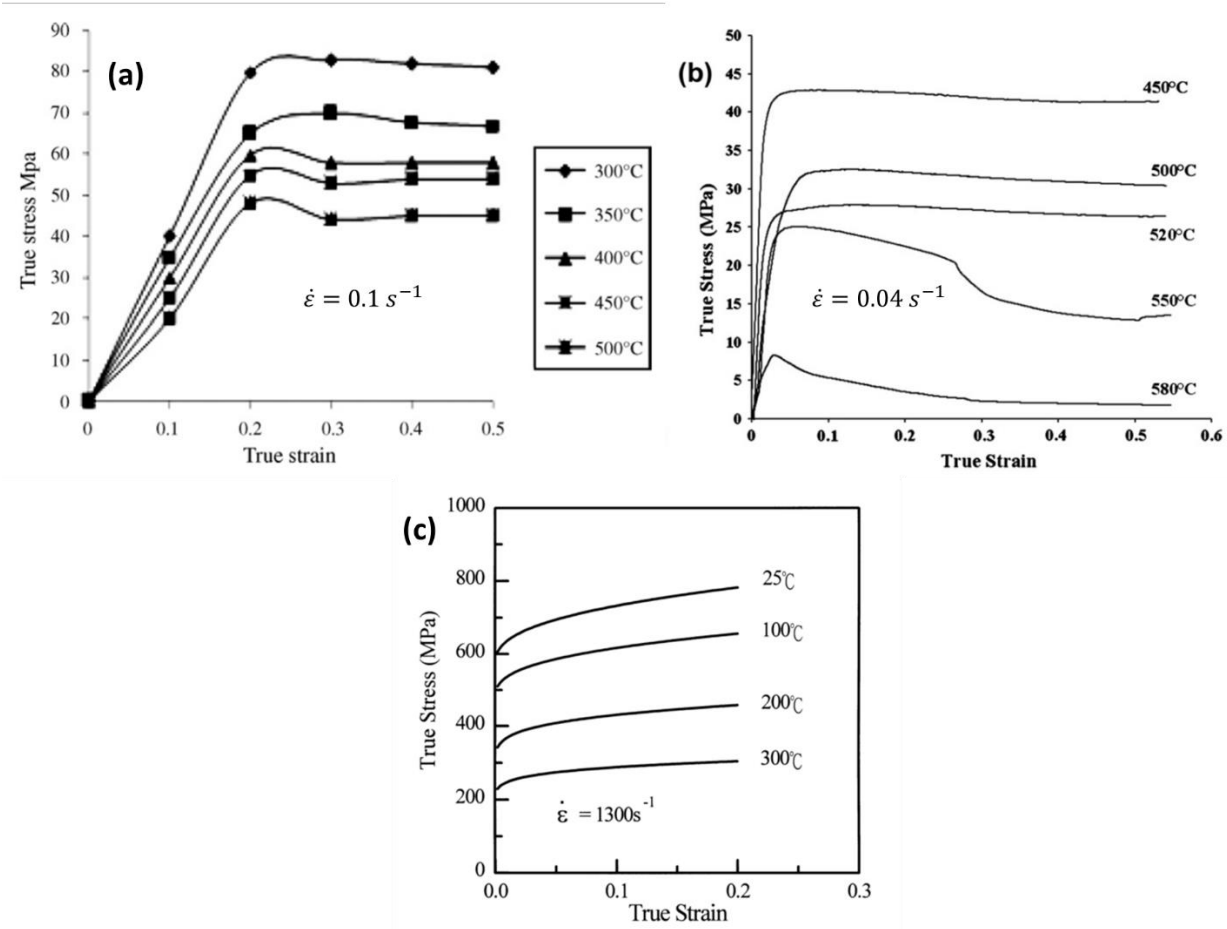

Figure 1. Stress-strain curves for AA7075 at elevated temperatures, obtained from (a) Rajamuthamilselvan and Ramanathan [4], (b) Rokni *et al.* [5] and (c) Lee *et al.* [30]

Chen *et al.* [31] performed elevated temperature tensile testing on AA7085, the results of which are shown in Figure 2. Their method involved solutionizing the material and then water quenching it. The quenching was then followed by heating the material and then deforming it at that elevated temperature. Wang *et al.* [32] tested AA7075 in which they did incorporate a quenching apparatus. However, their study made no use of digital image correlation (DIC) techniques for accurate measurement of local strains during testing. To-date, there is no study in which the constitutive properties and local strains of a 7000-series alloy have been measured under conditions representative of die quenching.

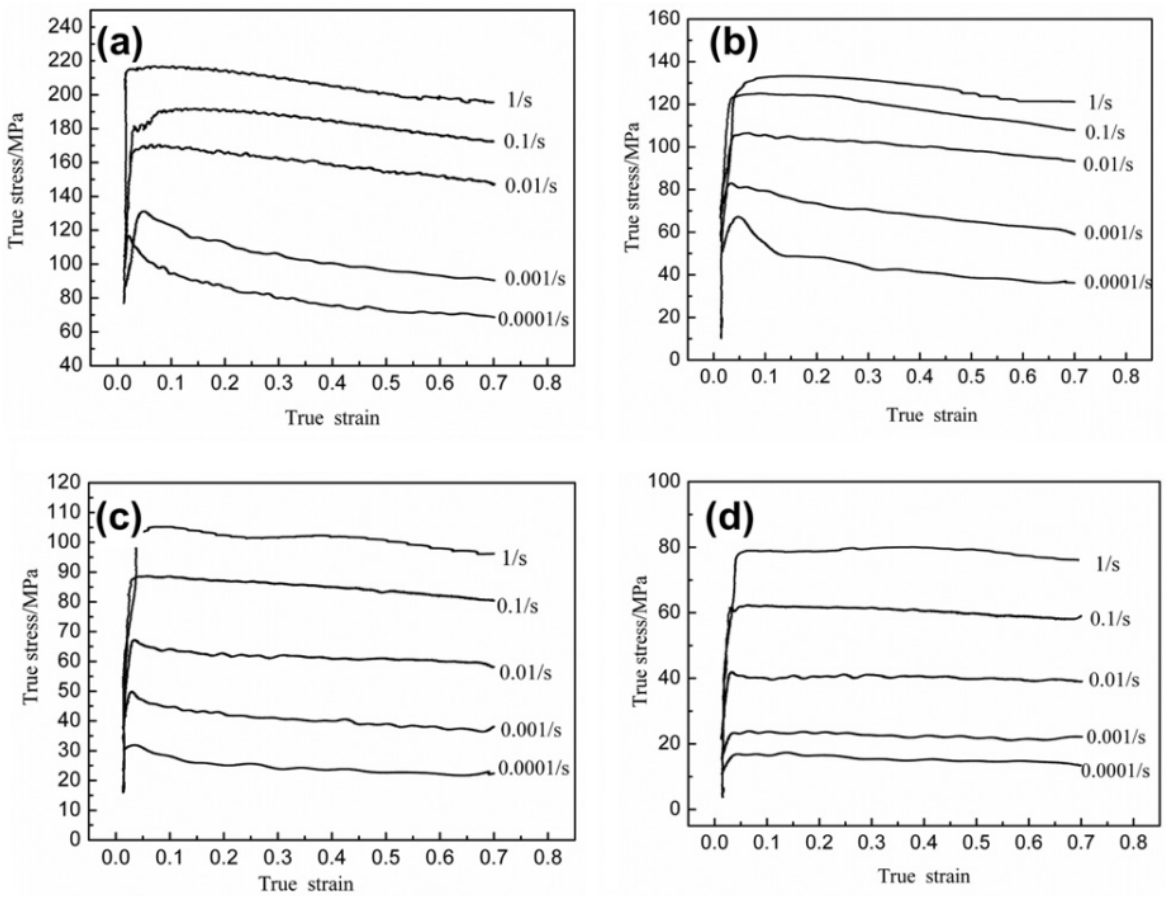

Figure 2. Stress-strain curves for AA7085 at elevated temperatures, obtained from Chen *et al.* [31] for (a) 300 °C, (b), 350 °C, (c) 400 °C and (d) 450 °C.

2.2.2. Strain Rate Dependent Constitutive Properties

AA7075 in its T6 temper is not particularly sensitive to strain rate at room temperature [33]. Most aluminum alloys, in general, tend not to exhibit a high strain rate sensitivity at room temperature [34–37]. They do, however, exhibit significant rate sensitivity at elevated temperatures [38], as a result of the thermal activation caused by higher temperatures [39,40]. Several studies, which were discussed in the previous section, have examined the elevated temperature strain rate sensitivity of AA7075 [4,5,30] and AA7085 [31].

Several approaches have been employed to capture the effect of strain rate and temperature sensitivity on the work hardening rate of aluminum alloys. One such model is the Johnson-Cook model used by Smerd *et al.* [34] to model AA5182 and AA6111 at elevated temperatures:

$$\sigma = (A + B\varepsilon^n)(1 + C\ln\dot{\varepsilon})\left(1 - \left(\frac{T - T_{room}}{T_{melt} - T_{room}}\right)^m\right) \quad \textbf{Eq. 1}$$

where A, B, C, m and n are parameters to be determined. Another model is the extended Voce model used by Rahmaan *et al.* [41]:

$$\sigma = A + (B + C\varepsilon)(1 - \exp(-D\varepsilon)) \quad \textbf{Eq. 2}$$

where A, B, C and D are parameters (different from those in Eq. 1) to be determined using experimental data, and are a function of temperature, T, and strain rate, $\dot{\varepsilon}$.

2.2.3. Anisotropy

Most aluminum alloys tend to exhibit anisotropy in their mechanical behaviour. The anisotropy of various aluminum alloys has been documented extensively in the literature [1,33,42–45]. Two types of anisotropy commonly considered are anisotropy in the yield stress *versus* anisotropy in strain ratios (*i.e.*, the ratio between the sheet thickness and width, also known as the r-value). AA7075 tends not to exhibit significant anisotropy in its measured stress levels or hardening response; however, there is significant anisotropy in terms of the measured r-values [1,2,45]. The same statement is true for AA7085 [46] and AA7050 [47]. Figure 3 shows the anisotropic properties of AA7075.

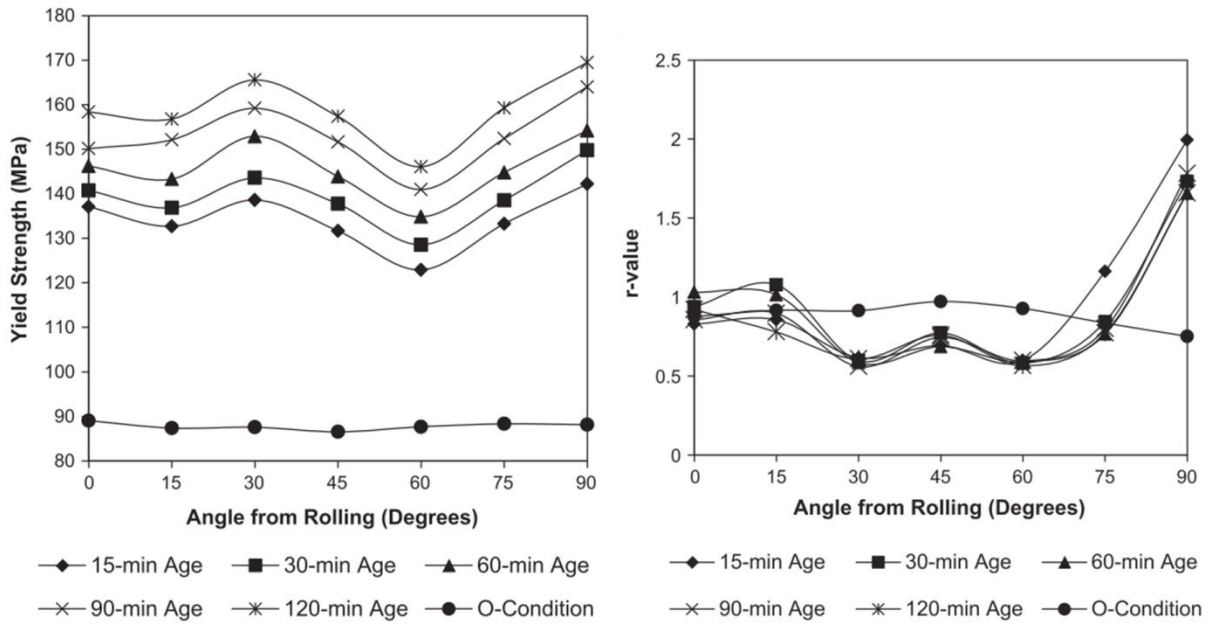

Figure 3. Anisotropic properties of AA7075, as a function of natural aging times [45].

To properly capture the anisotropic behavior, for the purpose of numerical simulation of the DQ process, an appropriate yield surface is required. The commonly used von Mises surface is isotropic and not sufficient to capture the directional anisotropy of these alloys. In their review paper, Toros *et al.* [48] wrote extensively about the different yield surfaces that have been used to model the constitutive response of various aluminum alloys. Ozturk *et al.* [42] used a Hill-90 [49] and a Barlat-89 [50] yield surface to capture the anisotropy of an AA6061-O sheet. More recently, Barlat *et al.* [51] proposed a plane stress yield function, which they devised specifically for aluminum sheets. The function relies on eight input parameters $\alpha_1 - \alpha_8$ in addition to the a exponent. Rahmaan *et al.* [52] calibrated a Barlat Yld2000 function for the room temperature behaviour of AA7075-T6 and AA7xxx-T76, which are shown in Figure 4. Other yield functions are also shown in the figure.

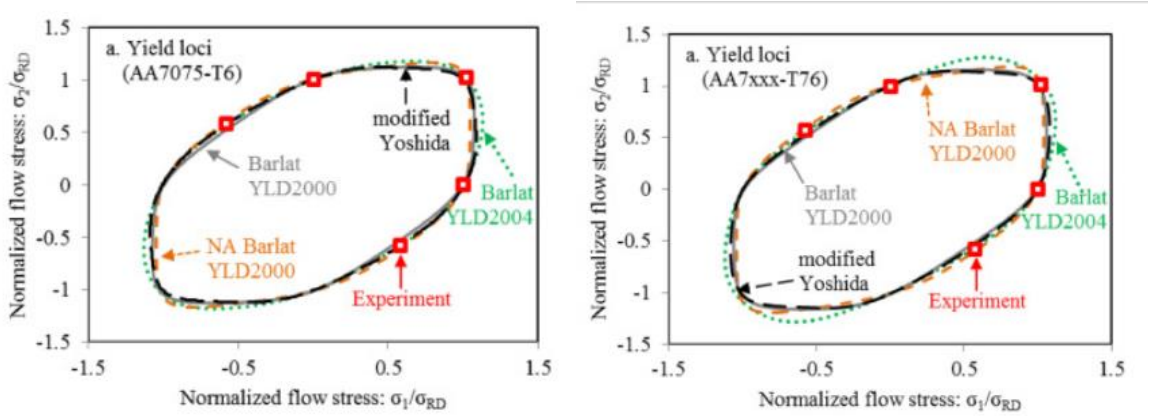

Figure 4. Various yield functions functions for AA7075-T6 and AA7xxx-T76 calibrated by Rahmaan *et al.* [52].

Tajally and Emadoddin [1] examined the anisotropy of AA7075 for temperatures ranging from 250-450 °C. They did not observe a significant change in anisotropy with respect to temperature. Several other studies have also concluded that aluminum alloys generally do not exhibit temperature-dependent anisotropy. Examples of such studies include Khan and Baig [53] for AA5182, Abedrabbo *et al.* [54] for AA3003, Abedrabbo *et al.* [44] for AA5182 and AA5754 and Li and Ghosh [38] for AA5182, AA5754 and AA6111.

2.3. Heat Transfer Coefficient (HTC)

A key material property required to simulate DQ operations is the operative heat transfer coefficient (HTC) between the blank and die, since this parameter controls the rate of heat extraction (cooling rate) during quenching. Malinowski *et al.* [55] devised a technique to characterize the heat transfer coefficient (HTC) in a metal forming procedure, as a function of die temperature and pressure. Their technique consisted of an inverse finite element (FE) approach, whereby experimentally obtained temperature-time profiles were inversely fit to an appropriate HTC value. A similar approach was used by Tanner and Robinson [56]. Merklein *et al.* [57] used a similar experimental technique to determine HTC as a function of die temperature and pressure. Their results for the HTC of Usibor® 1500 A-S steel are shown in Figure 5.

Between a die pressure of 10 MPa and 30 MPa, the HTC was found to double in magnitude. Other recent HTC studies were conducted by Caron *et al.* [13,58], who offered further improvements in HTC characterization by considering the effect of signal delay in the thermocouples used to measure die temperatures.

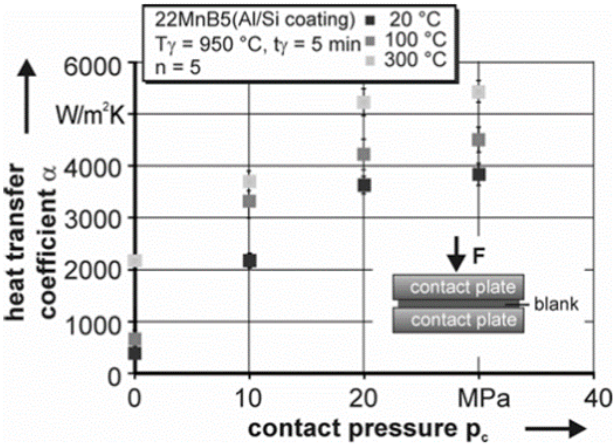

Figure 5. HTC as a function of die pressure and temperature, obtained from Merklein *et al.* [57].

For 7000-series aluminum alloys, there are fewer studies on HTC than for steel. Liu *et al.* [59] used an experimental technique, combined with FE models, to determine the HTC for AA7075. Tanner and Robinson [56] studied the HTC of AA7010 using experimental and analytical techniques.

2.4. Artificial Aging

In the realm of artificial aging, a longer aging time leads to greater strength in the material, until the peak aged (T6) condition is reached. After this point, the material begins to lose its strength, *i.e.*, overage, due to coarsening of precipitates and the potential change in the dislocation-precipitate interactions from shearing to by-passing [10,11,60]. According to Mahathaninwong *et al.* [11], peak aging for AA7075 starting in a quenched SSS state, at 185 °C occurs at approximately 2.5 hours. A similar result was obtained by Sevim *et al.* [61] for AA7075. Jabra *et*

al. [62] found that AA7085 overages quicker than AA7075, when both alloys are quenched and subsequently aged at 120 °C.

2.5. Models of Precipitate-Dislocation Interaction

2.5.1. Precipitation Hardening Models

A number of studies have sought to model the precipitation hardening of 7000-series alloys, and thereby predict the yield strength of the material after an aging treatment. Deschamps and Brechet [63] developed a model, based on Wagner and Kampmann [64] and the principles of precipitate nucleation, growth and coarsening. In addition, they proposed that yield strength is modelled considering the strength contributions of shearable and non-shearable precipitates, as well as the size distributions of those obstacles to dislocation movement. Another model was developed by Poole *et al.* [65], based on the modelling approach developed by Shercliff and Ashby [66] to predict the yield strength of AA7475 subjected to two-step aging treatments.

Esmaeili *et al.* [67–70] did extensive work examining the precipitation hardening behaviour of AA6111. They developed three models: (1) phase transformations during natural aging plus artificial aging, (2) phase transformations during a pre-aging followed by further artificial aging and (3) a model capable of predicting yield strength of the aforementioned aging treatments. Although these models were developed for 6000-series alloys, the underlying theory of precipitation kinetics can be applied to 7000-series alloys as well.

2.5.2. Models of Precipitate-Dislocation Interaction (Work Hardening Rate)

Deschamps *et al.* [14] investigated the stress-strain and work hardening response of AA6111 and a 7000-series alloy that were subject to different aging conditions. They found the work hardening rate (WHR) of the as-quenched AA6111 in its supersaturated state is very high, and it

further increases with natural aging for six months. The WHR of the Al-Zn-Mg alloy, naturally aged for three days, was also reported to be high, while the WHR for both alloys reduced with artificial aging. In general, work hardening rate is reduced as the extent of artificial aging is increased [71,72].

Cheng *et al.* [73] proposed the following equation to account for the interaction between precipitation hardening and dislocation accumulation (plastic work) based on their work on AA6111 and AA7030:

$$\sigma_{flow} = \sigma_{ss} + \left(\sigma_{ppt}^{n} + \sigma_{dis}^{n}\right)^{1/n} \quad \textbf{Eq. 3}$$

where σ_{ss} represents the yield strength of the material in its SSSS. σ_{ppt} and σ_{dis} are the strength contributions due to precipitation hardening (aging) and dislocation accumulation (work hardening), respectively, and exponent *n* describes their interaction. Fazeli *et al.* [74] used Eq. 3 to devise a model capable of predicting the flow stress of an Al-Mg-Sc alloy. Their model was able to accurately capture the plastic stress-strain response of the Al-Mg-Sc alloy subjected to different aging treatments. Generally, σ_{ss} in Eq. 3 can be obtained experimentally through a single tensile test, while σ_{ppt} and σ_{dis} need to be calculated using additional experimental data and/or theoretical/empirical formulations. To determine σ_{dis}, Fazeli *et al.* [74] proposed integrating the work hardening rate caused by the increase in dislocation density, as follows:

$$\theta_{dis} = \theta_0 \left(1 - \frac{\sigma_{dis}}{\sigma_s}\right) + \frac{K_{ppt} f}{\sigma_{dis} \bar{R}} \quad \textbf{Eq. 4}$$

where θ_{dis} is the work hardening rate caused by increase in dislocation density, θ_o is the total WHR at the yield point, and K_{ppt} and σ_s are fitting parameters to be determined from

experimental data. $\bar{R}$ is the average precipitate radius and f is the volume fraction of precipitates. Both of these parameters need to be determined through experimental analysis. When combined, the three terms in Eq. 3 provide a useful framework for determining the flow stress behaviour of an aluminum alloy based on its aging treatment.

2.6. Summary of the Relevant Literature

Several studies have examined the parameters (from a materials processing point of view) required to solutionize and quench 7000-series alloys and subsequently age them. Most of the current literature pertaining to process parameters does not put emphasis on the requirements of a metal forming operation such as die quenching.

There are two shortcomings within the current literature from a constitutive characterization perspective: (1) the quenching cycle in the DQ process is not replicated (*i.e.* the material is not tested in a solutionized condition) and (2) the post-necking behaviour is not properly analyzed. Another shortcoming in literature is that HTC data is not available for 7000-series alloys, other than studies by Liu *et al.* [59] and Tanner and Robinson [56] which are based on inverse modelling.

In regards to modelling post-die quenching properties (*i.e.*, after an aging treatment), no model exists that is capable of predicting the stress-strain response of a 7000-series alloy after a variety of aging treatments. Esmaeili *et al.* [67–70] have developed models that can predict the yield strength of 6000-series alloys and may be applicable to 7000-series alloys [75]. The precipitate-dislocation models proposed by Cheng *et al.* [73] and Fazeli *et al.* [74] for the prediction of WHR may be appropriate for use with the 7000-series alloys in the current study.

3. Objectives and Scope

3.1. Research Objectives

The overall aim of the research presented herein is to determine optimal die quenching and aging process parameters and to develop predictive models of the die quenching process and subsequent mechanical properties suitable to support development of automotive structural components. Two alloys are studied: AA7075 because of its widespread usage in the published literature and a developmental 7000-series alloy (referred to as AA7xxx) because of its lower sensitivity to quench rate (owing to its higher zirconium content compared to AA7075 [21]). The chemical compositions for each alloy are shown in Table 1.

Table 1. Chemical composition for AA7075 (measured) and AA7xxx alloy (nominal) [76].

Elements	**AA7075**	**AA7xxx**
Aluminum	90.07%	87.6-90.4%
Zinc	6.35	7.0-8.0
Magnesium	1.92	1.2-1.8
Copper	1.46	1.3-2.0
Zirconium	Negligible	0.08-0.15
Iron	0.10	0.08
Chromium	0.10	0.04

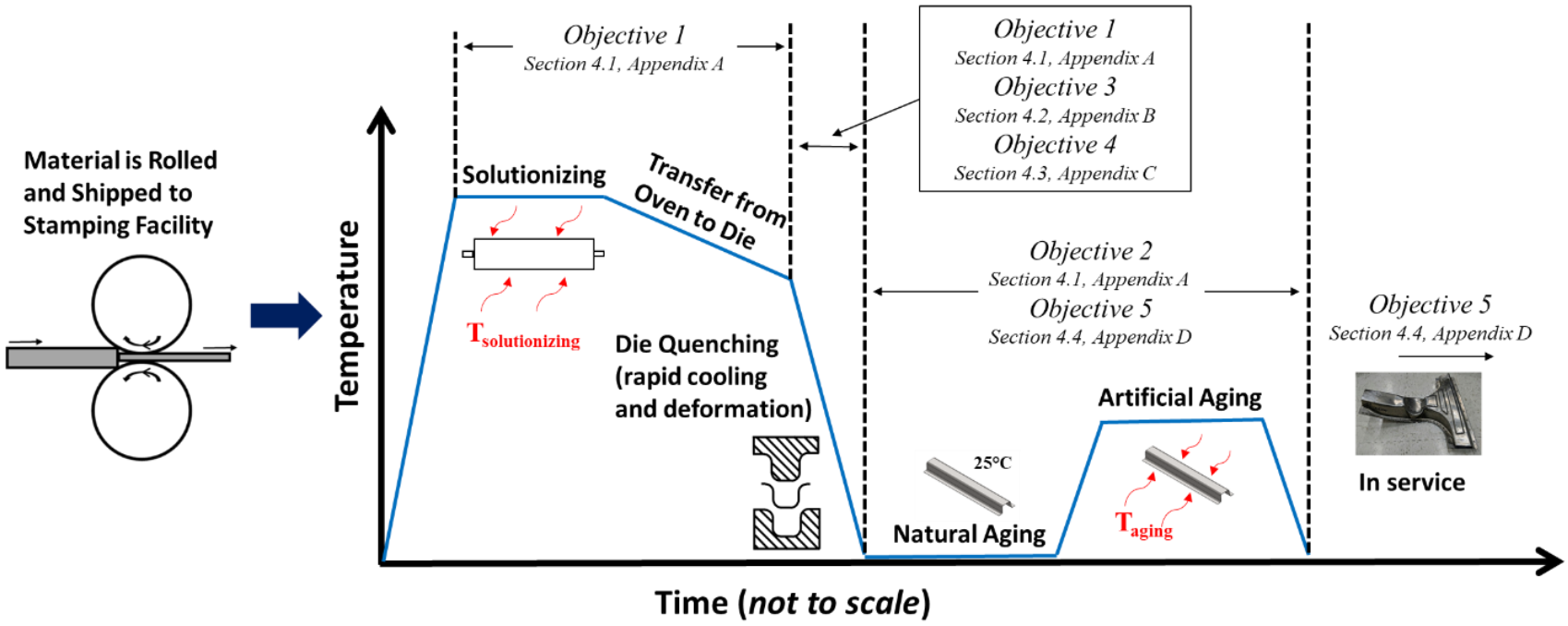

Figure 6. Schematic of the DQ process chain, showing positioning of each objective in this thesis.

Figure 6 shows a schematic of the DQ process chain spanning material supply through as-die quenched (in-service) final properties. In order to address the gaps in current knowledge identified in the literature review, a series of five research objectives were defined for this thesis, as listed in the following. The positioning of the research objectives within the process chain is also indicated in Figure 6.

Objective 1: Characterize the effect of DQ processing parameters (solutionizing time, transfer time and quench rate) on subsequent aging response;

Objective 2: Characterize the effect of multi-step aging treatments, that include the effect of the automotive paint bake cycle (PBC) (177 °C for 30 minutes), on final mechanical properties, targeting T6 and T76 tempers;

Objective 3: Develop and validate a constitutive model that can predict the stress-strain and anisotropic response of both alloys during the DQ process;

Objective 4: Calculate the HTC of both alloys during die quenching as a function of contact pressure;

Objective 5: Experimentally analyze the stress-strain behaviour and develop a model, based on the theories governing precipitate-dislocation interactions, to predict the WHR for single and multi-step aging treatments.

3.2. Scope of Work

To address objective 1, a parametric study was undertaken comprising a series of die quenching experiments in which the solutionizing time, transfer time and quench rate were varied. The effect that each parameter had on the age hardenability of the quenched material was assessed using hardness and/or tensile tests. For objective 2, a similar experimental programme was undertaken in which as-die quenched material was subjected to various artificial aging treatments that included an automotive paint bake cycle as a final aging step. A set of artificial aging treatments was identified that resulted in final properties similar to a conventional T6 or T76 temper. Note that a T76 (slightly over-aged) temper is often desirable to impact improved

resistance to stress corrosion cracking [61]. Section 4.1 summarizes the results of these aspects of the work, while the research article in Appendix A provides a more in-depth discussion.

To devise a constitutive model for the DQ process (Objective 3), tensile and shear experiments were conducted at various temperatures and strain rates. A custom quenching apparatus was built to apply the temperature-time cycle of a DQ process onto the test specimens. The stress-strain curves were obtained using a novel technique, called the area reduction method (ARM), that approximates the cross-sectional area of the diffuse neck in the tensile specimen using stereoscopic digital image correlation (DIC). The anisotropy of the two alloys was also characterized and a Barlat Yld2000 surface [51,77] was calibrated. Finally, the constitutive model was then applied to model a die quenching deep draw operation and the predicted results were compared with experiment. A summary of these results is provided in Section 4.2 and the research article in Appendix B provides greater detail.

A key boundary condition required to accurately model the DQ process is the operative heat transfer coefficient under DQ conditions (Objective 4). To obtain the HTC, a series of instrumented flat die quenching experiments were performed and the HTC was determined as a function of contact pressure. The methodology to calculate HTC as a function of contact pressure is summarized in Section 4.3 and a detailed presentation of the experiments is discussed in the paper in Appendix C.

The final properties of AA7075 after die quenching and artificially aging were addressed by Objective 5. Of particular interest was the manner in which the two primary strengthening mechanisms, precipitation hardening and work hardening. To this end, a micro-mechanics based model was devised to predict the work hardening rate (WHR) and flow stress of AA7075 after an

artificial aging treatment is applied. Section 4.4 and Appendix D provide a description of this model and the supporting experiments.

4. Results and Discussion

A summary of the results obtained from this research is given in this chapter of the thesis synopsis. Appendices A-D provide more in-depth discussion of the methodology and the results. Each appendix consists of a journal article that has either been peer-reviewed and published or submitted to a relevant journal in the research field. The four appendices are:

Appendix A	Omer K, Abolhasani A, Kim S, Nikdejad T, Butcher C, Wells M, Esmaeili S, Worswick M. Process parameters for hot stamping of AA7075 and D-7xxx to achieve high performance aged products. Journal of Materials Processing Technology 2018;257:170–9. doi:10.1016/j.jmatprotec.2018.02.039.
Appendix B	Omer K, Butcher C, Esmaeili S, Worswick M. Characterization and application of a constitutive model for two 7000-series aluminum alloys subjected to hot forming. International Journal of Mechanical Sciences 2020;165. doi:https://doi.org/10.1016/j.ijmecsci.2019.105218.
Appendix C	Omer K, Butcher C, Worswick M. Characterization of heat transfer coefficient for non-isothermal elevated temperature forming of metal alloys. International Journal of Material Forming 2019. doi:10.1007/s12289-019-01478-3.
Appendix D	Omer, K., Abolhasani, A., Esmaeili, S., Worswick, M., A Microstructure-Based Model to Predict the Stress-Strain Behaviour of AA7075 Following Various Aging Treatments. *Manuscript in preparation for journal submission*.

4.1. Effect of DQ Process Parameters and Aging Treatments

As discussed in Section 2.1, the solutionizing time, quench rate and transfer time during die quenching can have a significant effect on the subsequent age hardenability of the quenched material. To assess the effects of these three process parameters, an experimental programme was devised, which is outlined below. Custom artificial aging treatments were also investigated. Note that Appendix A provides greater detail concerning the methodology and results of this aspect of the research.

4.1.1. Methodology

The experiments were performed using a convection furnace and a pair of flat dies mounted in a hydraulic press. The dies are shown in Figure 7a. The blank measured 125 x 125 mm with a cutout at its centre. A thermocouple was attached inside the cutout, as shown in Figure 7b. To investigate the first processing parameter, *i.e.*, the solutionizing time, blanks were placed in the furnace for 2.5, 5, 8, 15 or 30 min in total. The blanks were subsequently quenched in the flat dies at an average quench rate of 56 °C/s. Hardness measurements were taken 24h and 3 weeks after the quench, in order to track the amount of natural aging over time, and therefore, judge the age hardenability of the quenched samples.

For the second processing parameter, two transfer times were investigated: 6s and 15s. Tensile specimens were solutionized and quenched at a rate of 56 °C/s and tensile tests were performed within 10 minutes of quenching and after six days of natural aging.

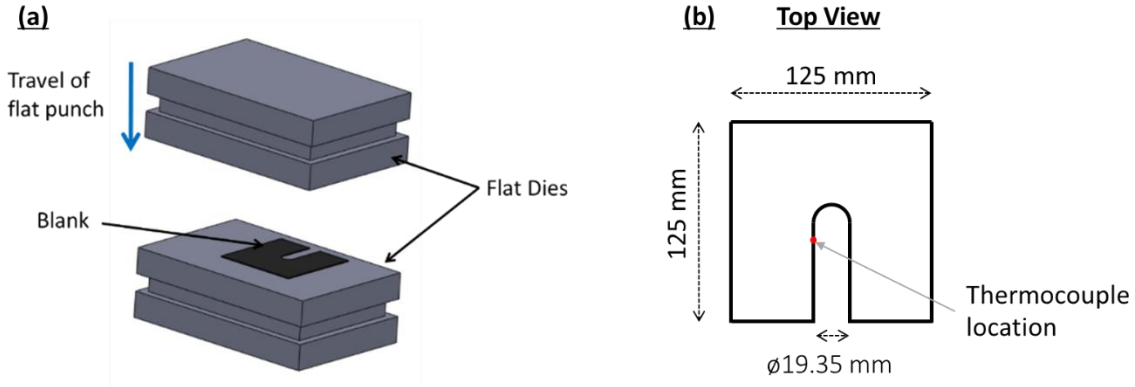

Figure 7. (a) Flat dies used to quench the aluminum blanks. Details of the die geometry can be found in Caron *et al.* [13]. The dies were made out of tool steel [76], and (b) a schematic of the blank and the thermocouple location (for experiments where a thermocouple was used).

The third processing parameter, *i.e.*, quench rate, was investigated by heating the blank for 8 min, transferring it to the die (within 6s), and quenching at 27, 34, 40, 56 or 128 °C/s. The quench rate was controlled by varying the die pressure since HTC is a direct function of contact pressure

(see Section 4.3). Hardness measurements were conducted 15 min, 24h and three weeks after the quenching process.

For aging treatments on AA7075, a standard "T6 treatment" (121 °C for 24h) was adopted as a baseline. Experiments were also performed considering a two-step aging treatment in which specimens were aged at the T6 temperature of 121 °C for 4, 8 and 12h, followed by a paint bake cycle (PBC) comprising 177 °C for 30 min. These modified aging treatments are referred to as "interrupted T6-paint bake" or T6IPB and the goal in considering these treatments was to reduce the T6 aging period by considering the effect of the PBC. Tensile tests were performed on each interrupted treatment to compare its performance against the T6 temper. For AA7xxx, standard T6 and slightly over-aged T76 treatments and a corresponding "interrupted" schedule incorporating the PBC were considered, as outlined in detail in Appendix A.

4.1.2. Results

A total solutionizing time of 8 min was found to be sufficient for both AA7075 AA7xxx. The total time of 8 min corresponds to a *soak time* of 90s at the solutionizing temperature of 470 °C. It should be noted that the AA7075 material in this work was received in a T6 temper and the AA7xxx material in a T76 temper. Other starting tempers may, in fact, require a longer or shorter time for proper solutionizing.

The effect of transfer time on subsequent aging response can be seen in Figure 8 which shows engineering stress-strain curves obtained from the tensile tests on samples that were subjected to 6 and 15s transfer times. Also plotted in Figure 8 are the UTS, yield strength and total elongation as a function of transfer time. The longer transfer time did not have a strong effect on the work hardening response for either alloy. AA7075, however, did exhibit a decrease in elongation when

a transfer time of 15s was used (compared to 6s) whereas the elongation of the developmental AA7xxx did not change for these two transfer times.

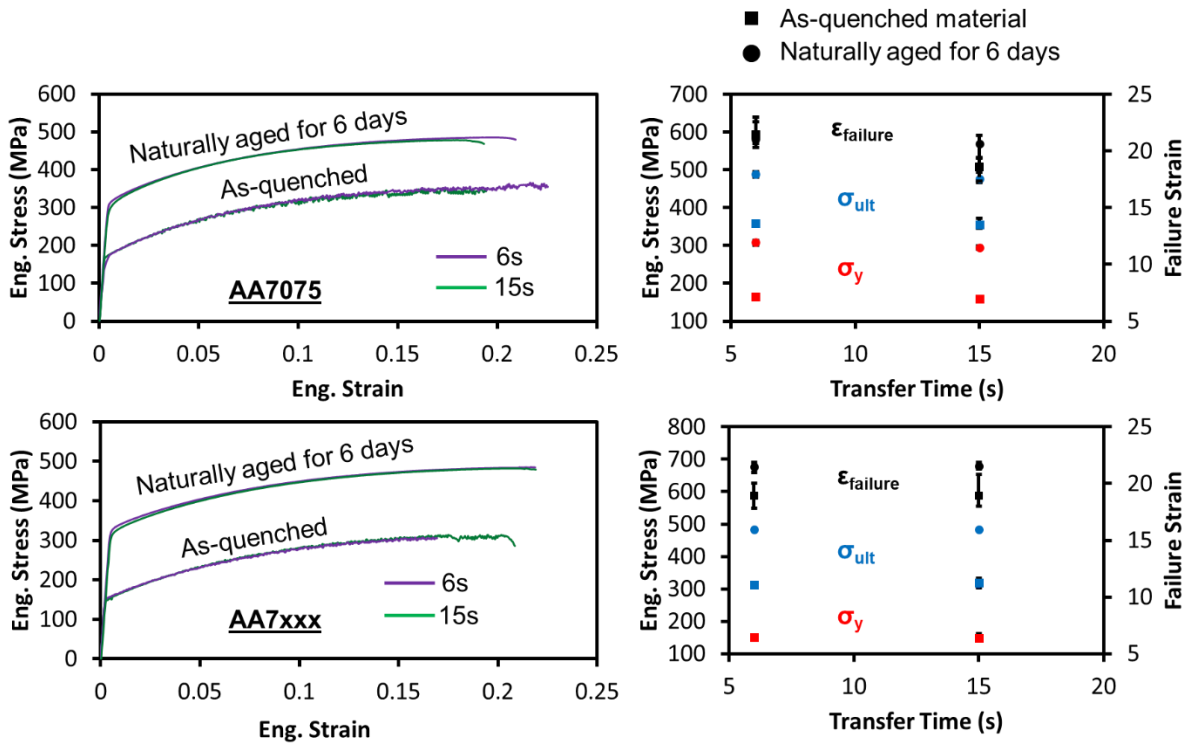

Figure 8. Engineering stress-strain curves for different transfer times, and also the yield strength, UTS and total elongation as a function of transfer time. The material was solutionized, quenched at 56 °C/s and then tensile tested [76].

Figure 9 serves to examine the effect of quench rate and shows Vickers hardness as a function of quench rate. The hardness measurements show that the natural aging of as-quenched AA7075 is strongly linked to quench rate. The AA7075 specimens quenched at or above 40 °C/s, exhibited a hardness of 145-150 HV after quenching and three weeks of natural aging. For the lower quench rates (27 and 34 °C/s), the AA7075 samples exhibited a lower hardness which is indicative of a lower precipitation hardening response. Interestingly, the AA7075 samples quenched at 27 and 34 °C/s exhibited higher hardness levels immediately after quenching compared to samples quenched at higher rates. The higher hardness after immediately after quenching is attributed to premature precipitation at grain boundaries [78] during the DQ process

which results in the lower subsequent natural aging response and lower elongation. The AA7xxx alloys were insensitive to quench rate for the range of experimental conditions, demonstrating an attractive, lower quench sensitivity compared to AA7075.

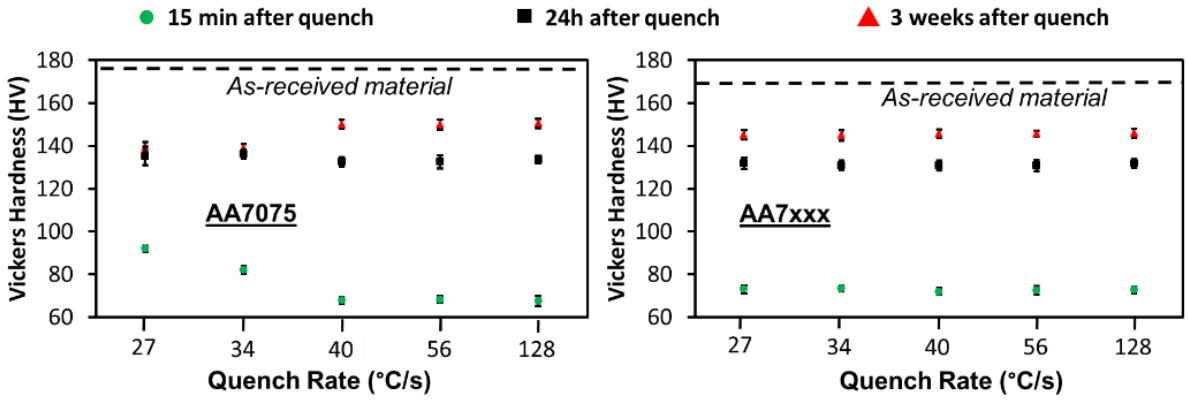

Figure 9. Hardness measurements of quenched materials at different cooling rates [76].

The effect of multi-step aging on the stress-strain response of AA7075 is shown in Figure 10, along with the as-received T6 temper response. From the data, it is evident that a 4h first step age at 121 °C followed by a PBC results in an under-aged condition, whereas the 8h first step age produces a strength that matches the as-received T6 condition. Interestingly, the 12h first step age results in an over-aged condition after PBC, as reflected in the loss in strength. Based on these results, the 8h first step aging at 121 °C, followed by PBC, was adopted as the recommended process for automotive DQ processing of AA7075 and was designated the T6IPB temper for the purposes of this thesis.

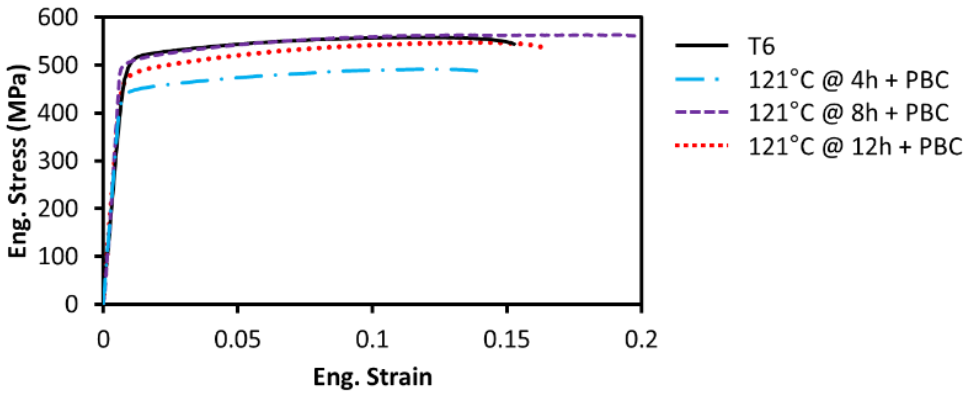

Figure 10. Measured stress-strain curves of AA7075 subjected to heat treatment at 121 °C for 4h, 8h and 12h, followed by a PBC. The stress-strain curve for a conventional T6 heat treatment is also shown for reference [76]. All tensile tests were conducted using a strain rate of 0.001 s^{-1}.

Figure 11 shows the stress-strain properties of the aging treatments investigated for the AA7xxx temper. For AA7xxx, two tempers were explored: T6 (24h at 121 °C [79]) and T76 (5h at 120 °C followed by 15h at 163 °C [80]). Hardness measurements were conducted on samples aged at various temperatures (100, 120, 135, 150 or 163 °C) and aging times (ranging from 0.5 to 24h) followed by a PBC. The hardness measurements revealed that properties resembling a T6 temper could be achieved if AA7xxx was aged at 3h at 120 °C, followed by a PBC (dubbed the T6IPB temper). The hardness measurements also demonstrated that an aging treatment of 4h at 100 °C followed by a PBC results in properties similar to a T76 temper (dubbed the T76IPB temper). Figure 11 shows the stress-strain properties of AA7xxx-T6 alongside AA7xxx-T6IPB and the AA7xxx-T76 temper alongside the AA7xxx-T76IPB temper.

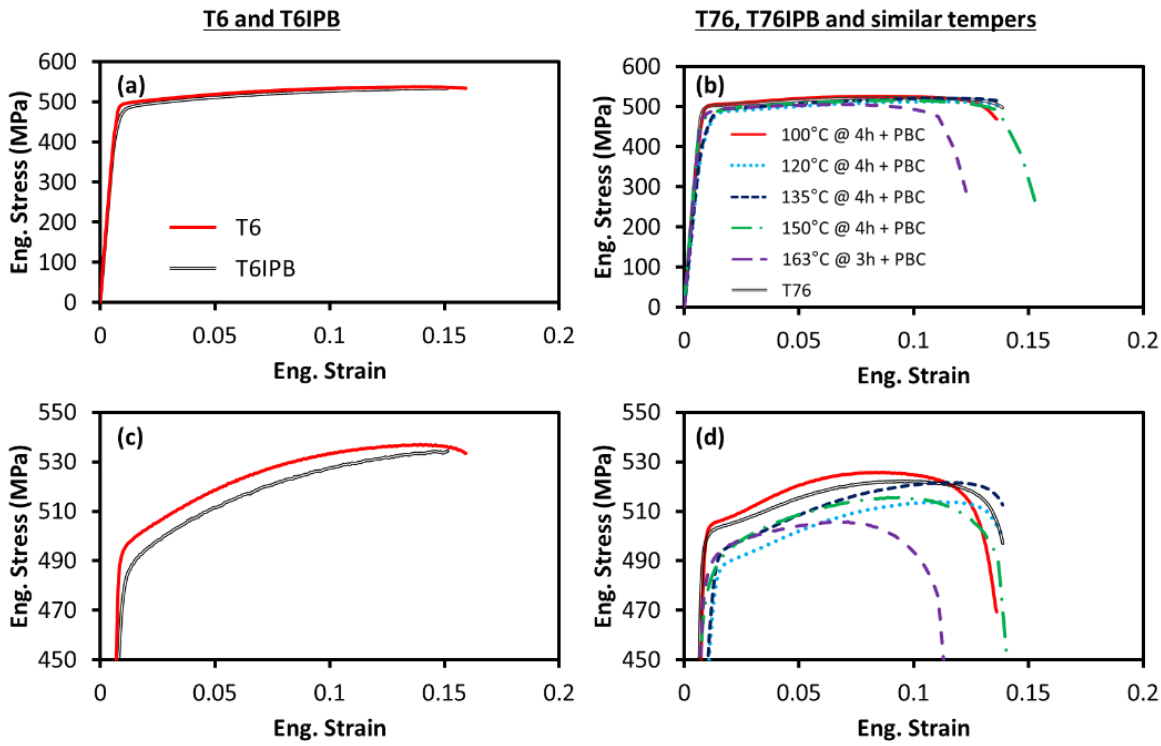

Figure 11. Stress-strain curves obtained from tensile tests for (a), (c) AA7xxx-T6 and -T6IPB, and (b), (d) several aging routes incorporating a PBC that yield in a hardness value similar to AA7xxx-T76. For reference, the T76 properties are also shown. Note that (c) and (d) are magnified views of (a) and (b), respectively [76]. All tensile tests were conducted using a strain rate of 0.001 s^{-1}.

The die quench processing and artificial aging parameters, determined from the experiments, that are required to achieve either T6 or T76 final properties for die quenched AA7075 and AA7xxx are shown in Table 2. In general, AA7xxx exhibited less quench rate sensitivity than AA7075 and also a higher tolerance to longer transfer time than AA7075. For both alloys, a total soak time of 90 s was found to be sufficient. Including the 6.5 min heat up time required in the furnace, a total solutionizing time of 8 min was determined.

Table 2. Processing parameters for the DQ of AA7075 and AA7xxx and subsequent aging treatments that can leverage the PBC. Note that T76 properties were not considered for AA7075.

Parameter	**AA7075-T6IPB**	**AA7xxx-T6IPB**	**AA7xxx-T76IPB**
Solutionizing Time	8 min	8 min	8 min
Solutionizing Temperature	470 °C	470 °C	470 °C
Minimum Quench Rate	56 °C/s	27 °C/s	27 °C/s
First Stage Artificial Aging Time	8h	3h	4h
First Stage Artificial Aging Temperature	121 °C	120 °C	100 °C
Paint Bake Cycle	177 °C for 30 min	177 °C for 30 min	177 °C for 30 min

4.2. A Constitutive Model to Simulate DQ Forming Processes

A key requirement to develop a constitutive model to simulate the DQ process is to characterize flow stress as a function of strain, strain rate and temperature while the material is in a fully solutionized condition at elevated temperature. This section presents results using a custom experimental device built to perform tensile testing immediately after rapidly cooling of tensile specimens from the solutionizing temperature (470 °C for 7000-series alloys) to the target test temperature. In addition, a novel post-processing technique, referred to as the Area Reduction Method" (ARM), was developed which accounts for the minimum cross section when determining the current true stress. Knowledge of the current true stress is important since, at elevated temperatures, these alloys satisfy the Considère criterion at very low strain levels and the majority of the deformation occurs under diffuse necking conditions. This section also presents a validation study in which the constitutive model was used to simulate a series of DQ deep draw experiments also developed as part of this research. A summary of these results is

presented herein and the reader is referred to Appendix B of this thesis for a more in-depth discussion of the constitutive model development and application.

4.2.1. Experimental Methodology

The tensile tests in this work were performed on a MTS Criterion 64 servo-electric tensile frame with hydraulic grips and an MTS 651 furnace, as shown in Figure 12. Tests were performed at 25, 115, 200, 300, 400 or 470 °C at three strain rates: 0.01, 0.1 and 0.5 s^{-1}.

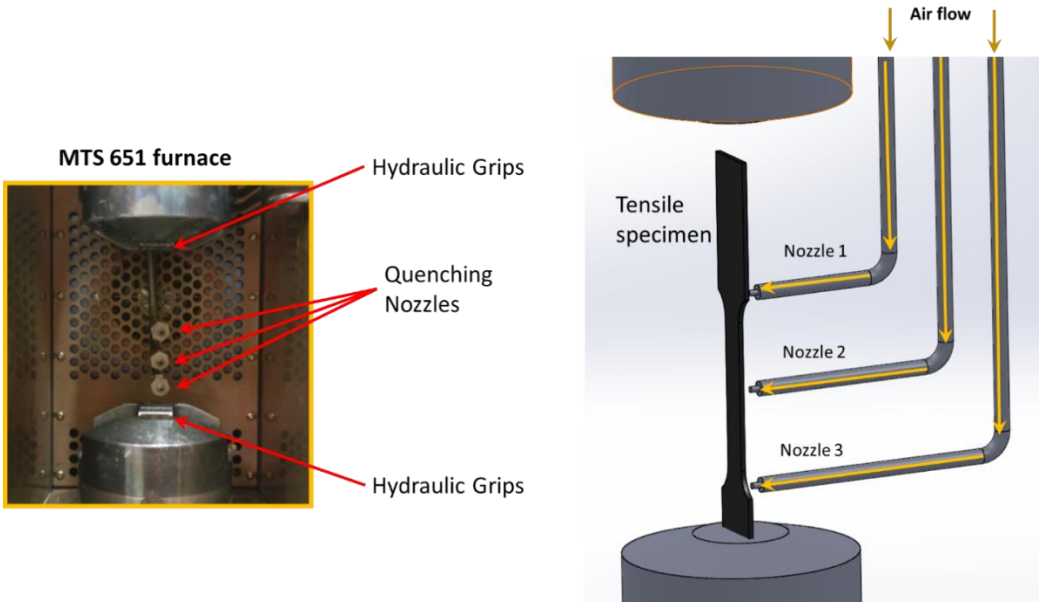

Figure 12. Experimental setup of the elevated temperature tensile tests. The quenching apparatus, consisting of three individual nozzles is also shown.

The tensile samples were placed in the furnace at 470 °C and held for eight minutes, which replicated the solutionizing stage of the DQ process. For test temperatures below 470 °C and above room temperature, the specimens were quenched after solutionizing using three air jets. The air jets (shown in Figure 12) directed cold air onto the tensile specimen from an Exair vortex chiller. Once the specimens cooled to the target test temperature, the tensile test was initiated. Section 3.1 in Appendix B contains more information on this setup, however, several typical temperature histories are presented in Figure 13 from which it can be seen that a high quench

rate and relatively constant test temperature was achieved. A minimum quench rate of 55 °C/s was achieved and a thermal gradient of no more than 7 °C was observed in the gauge region of the tensile specimen. A painted speckle pattern was applied to all tensile samples to support *in situ* digital image correlation (DIC) measurements of strain prior to solutionizing using Zynolyte® Hi-Temp paint. The DIC setup consisted of two Nikon AF Micro 180 mm lens, each of which was attached to a Point Grey GRAS-50S5M-C camera; further details concerning the DIC setup is provided in Section 2.1 of Appendix B.

The stress-strain behaviour was calculated for all target test temperatures and strain rates along the rolling direction (RD). In addition, the r-values were also characterized in three directions: rolling (RD), transverse (TD) and 45° (DD) at two temperatures: 25 and 470 °C. Finally, shear tests were performed for the purposes of yield surface calibration at 25 and 470 °C at 0.01 s^{-1}. The shear testing is discussed in Sections 2.4 and 5.2 of Appendix B.

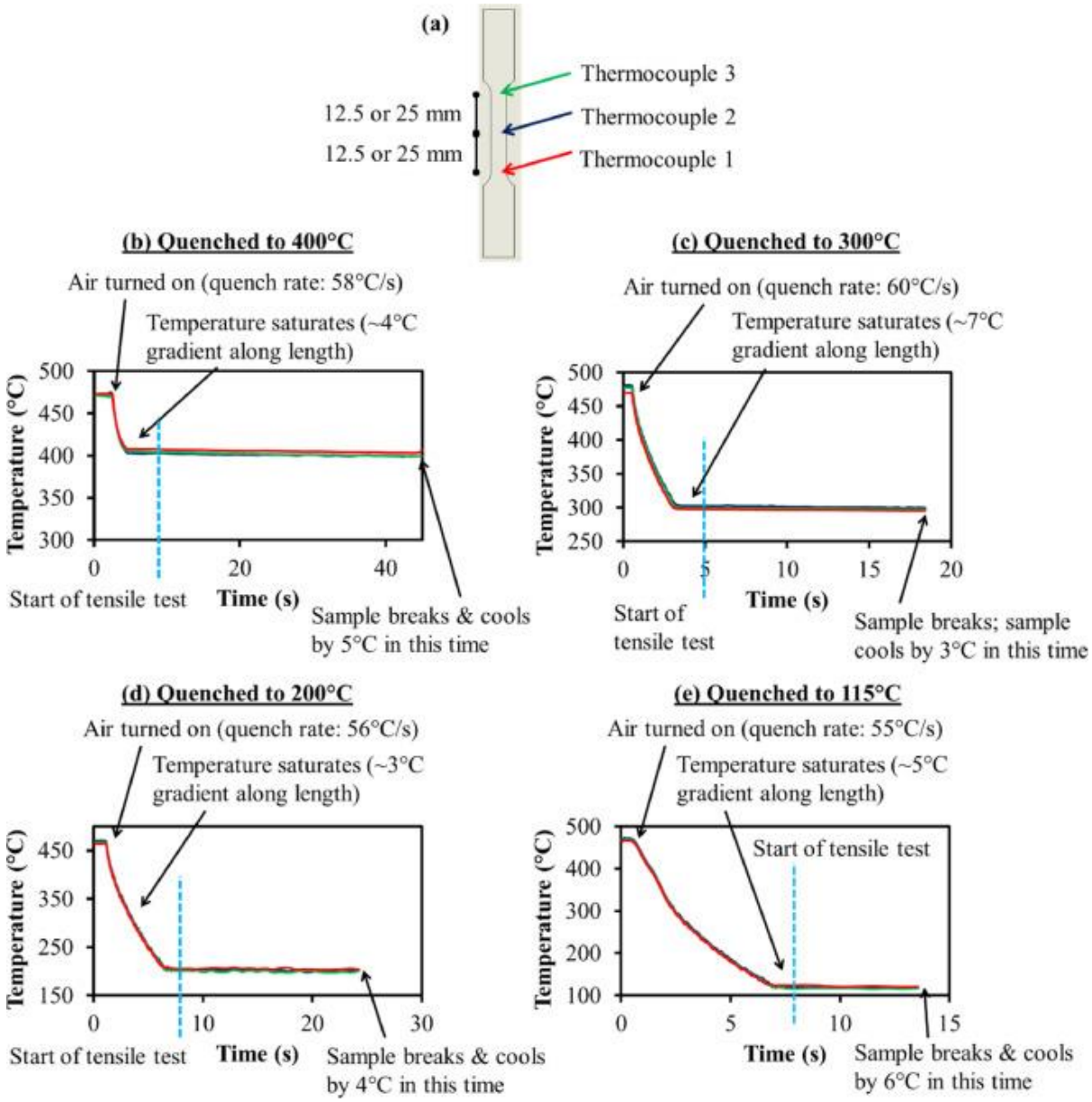

Figure 13. Temperature-time histories in some tensile specimens. (a) shows the thermocouple locations on the tensile frame and (b-e) shows the temperature-time history in samples tested at 400, 300, 200 and 115 °C, respectively. All of these curves are from tensile tests performed at a strain rate of 0.01 s^{-1}.

4.2.1.1. Area Reduction Method

To obtain true stress-strain curves, the ARM was used, in which experimental surface strain and displacement data is extracted from the DIC system during the tensile test. The data is extracted using a line slice across the cross-section of the diffuse necking zone. The surface geometry is

then utilized to approximate the area of the section as depicted in Figure 14. Further detail on the ARM is provided in Section 2.2 of Appendix B. Section 3.3 in Appendix B serves to confirm the accuracy of this method, demonstrating good agreement between cross-sectional areas calculated using the ARM and those measured under an optical microscope after testing.

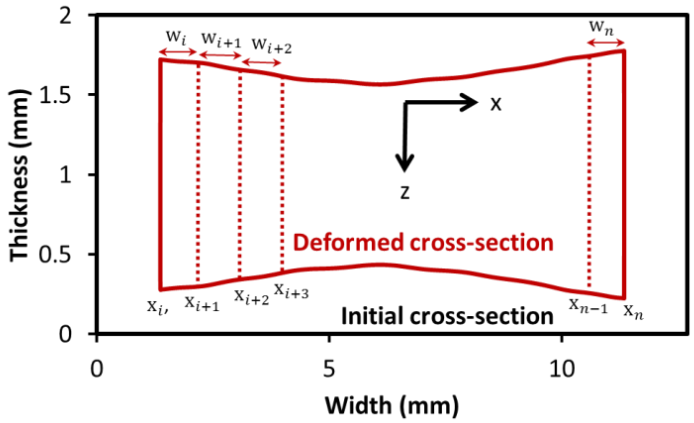

Figure 14. A reconstructed cross-section profile of an AA7075 sample using the ARM.

4.2.2. Results

4.2.2.1 Tensile Response

The true-stress strain curves obtained using the ARM are shown in Figure 15 for AA7075 and in Figure 16 for AA7xxx. Both figures also show a constitutive fit following the modified Voce model:

$$\sigma = A + \left(B + C\sqrt{\varepsilon^p}\right)(1 - \exp(-D\varepsilon^p)) \qquad \textbf{Eq. 5}$$

where A, B, C and D are phenomenological parameters dependent on temperature and strain rate. σ is effective stress and ε^p is effective plastic strain. In general, the agreement between model and experiment is quite good. The values of the constitutive parameters in Eq. 5 are reported in Table 3.

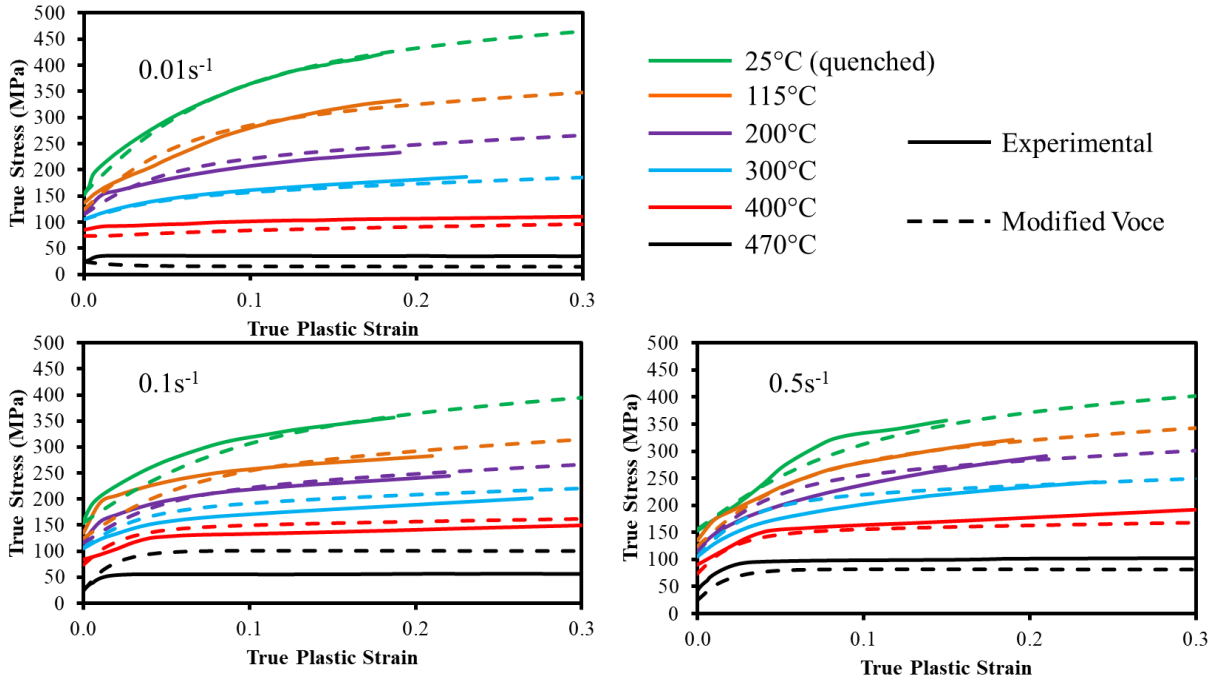

Figure 15. True stress-strain curves for solutionized AA7075 obtained using the ARM are shown as solid lines. The fit curves from the modified Voce model are also shown.

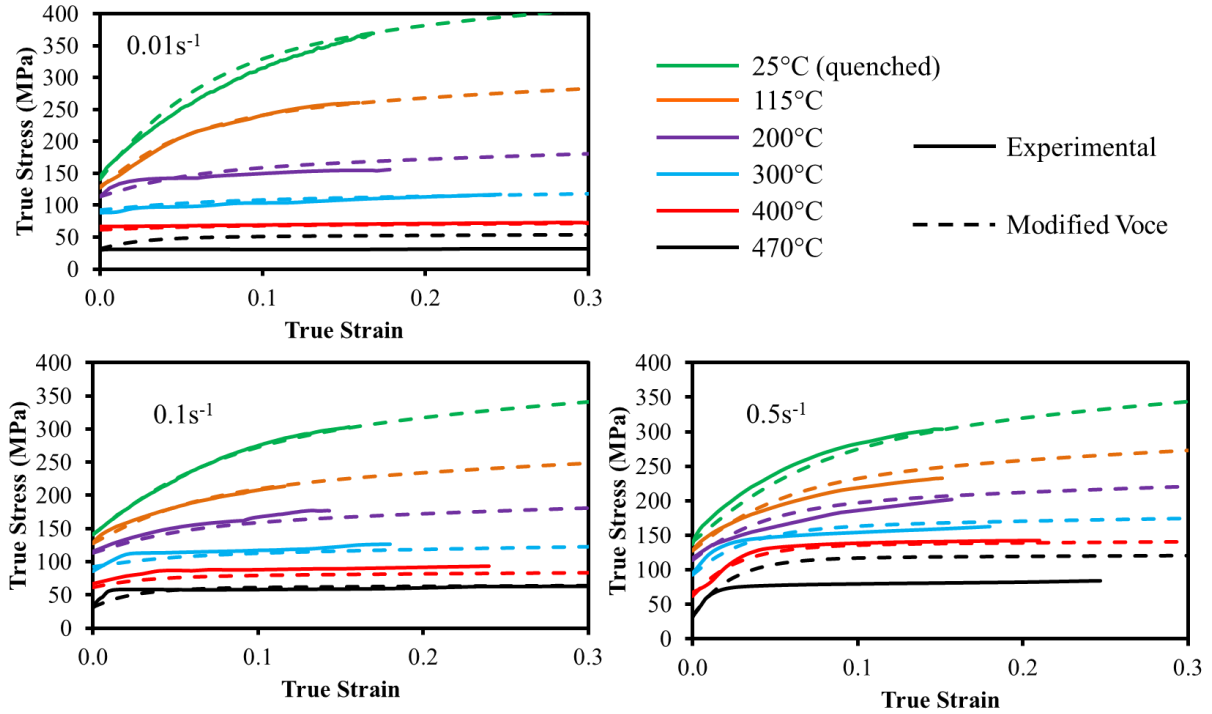

Figure 16. True stress-strain curves for solutionized AA7xxx obtained using the ARM are shown as solid lines. The fit curves from the modified Voce model are also shown.

Table 3. Parameters from the modified Voce equation for both alloys characterized where $\boldsymbol{T}$ is in Celsius.

Parameter	AA7075	AA7xxx
$\boldsymbol{A}$ **(MPa)**	$154.1 - 235.2T_r + 487.2T_r^2 - 381.7T_r^3$	$141.1 - 69.1T_r + 26.5T_r^2 - 66.7T_r^3$
$\boldsymbol{B}$ **(MPa)**	$1643\dot{\varepsilon}^2 - 961\dot{\varepsilon} + 186 + (83.8\ln\dot{\varepsilon} + 3.2)T_r + (-404.8\dot{\varepsilon} + 209.2)T_r^2$	$1527\dot{\varepsilon}^2 - 903\dot{\varepsilon} + 157 + (76.3\ln\dot{\varepsilon} - 58.8)T_r + (-42.8\ln\dot{\varepsilon} + 74.2)T_r^2$
$\boldsymbol{C}$ **(MPa)**	$251.3 - 142.5T_r - 113.5T_r^2$	$206.8 - 396.0T_r + 199.3T_r^2$
$\boldsymbol{D}$ **(mm/mm)**	$17.6 + 43.2T_r$	$20.5 + 25.0T_r$

4.2.2.2 Yield Surface Calibration

Table 4 shows the calculated r-values and standard deviation for both alloys at 25 °C and 470 °C, while Table 5 shows the corresponding stress ratios (ratios of yield strength in the TD and DD directions to yield strength along RD direction). The corresponding shear stress ratios (ratio of yield stress in shear to tensile yield strength along RD direction) are shown in Table 6. The r-values did not change significantly between the two values of temperature and neither did the stress ratios. Therefore, it was assumed that the yield surface shape (normalized with respect to RD yield stress) was invariant with respect to temperature.

Table 4. Calculated r-values and standard deviation for AA7075 and AA7xxx in the three directions tested.

AA7075	RD	DD	TD
25 °C (W-temper)	0.67 ± 0.03	0.93 ± 0.06	1.07 ± 0.05
470 °C	0.71 ± 0.07	0.90 ± 0.12	1.15 ± 0.11
AA7xxx	**RD**	**DD**	**TD**
25 °C (W-temper)	0.65 ± 0.04	1.41 ± 0.09	1.83 ± 0.21
470 °C	0.69 ± 0.06	1.60 ± 0.16	1.75 ± 0.27

Table 5. Calculated stress ratios for AA7075 and AA7xxx at 25 °C (W temper) and 470 °C

AA7075	RD/TD	RD/DD
25 °C (W-temper)	1.003	0.975
470 °C	1.023	0.975
AA7xxx	**RD/TD**	**RD/DD**

25 °C (W-temper)	1.004	0.988
470 °C	1.011	0.968

Table 6. Calculated shear ratios, and their standard deviations, for AA7075 and AA7xxx for the two temperatures and two directions tested. Note that the directions in this table refer to the principal direction of the stress.

AA7075	**RD**	**Specific Plastic Work (MPa)**	**DD**	**Specific Plastic Work (MPa)**
25 °C (W-temper)	0.578 ± 0.010	28.32	0.575 ± 0.012	27.55
470 °C	0.579 ± 0.005	1.26	0.575 ± 0.008	1.23
AA7xxx	**RD**		**DD**	
25 °C (W-temper)	0.586 ± 0.006	29.03	0.584 ± 0.009	28.64
470 °C	0.595 ± 0.012	1.33	0.596 ± 0.011	1.31

The measured stress ratios and r-values at room temperature were used to fit the coefficients of the Barlat Yld2000 [51] yield surface. The resulting yield *loci* are shown in Figure 17 for both alloys and the Barlat Yld2000 coefficients are provided in Table 16 of Appendix B. The yield surface calibration assumed isotropic stress-strain behaviour and strain path changes were not considered.

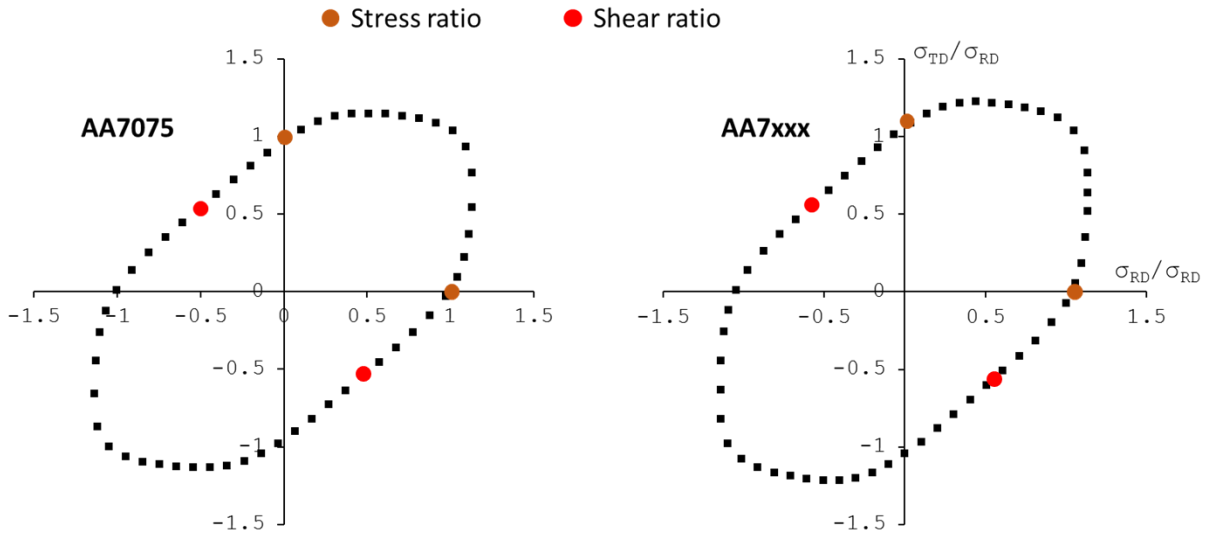

Figure 17. Normalized shapes of the yield surfaces for AA7075 and AA7xxx.

4.2.3. Model Validation - Application to DQ Deep Draw Operation

To assess the constitutive fits and the calibrated yield surfaces, FE models were developed of a series of DQ deep drawing experiments performed on a hydraulic press. The experiments were modelled using the LS-DYNA [81,82] commercial finite element code.

The deep draw procedure began by placing the blank in a convection furnace for 8 minutes at 470 °C. After 8 minutes, the blank was transferred manually into the press where it was placed on the die surface. The transfer time took 5s. The blank rested on lifter springs for another 5s prior to application of the binder load of 20 kN. The ramp up time for the binder load was 0.5s. Therefore, a total of 10.5s elapsed before the deep draw operation began. The punch velocity used was 10 mm/s. Two circular blank sizes were tested: 177.8 mm and 203.2 mm diameter. Five repeats were conducted for each alloy and blank size.

To measure the earring profiles, each formed cup was placed on an Epson Perfection V30 scanner. A circle of constant radius was drawn around the profile of the drawn cup on the scanned image, as shown in Figure 18. The distance from the circumference of the circle to the edge of the cup was measured using Matlab. The Matlab program used to analyze the cups was developed by Noder [83].

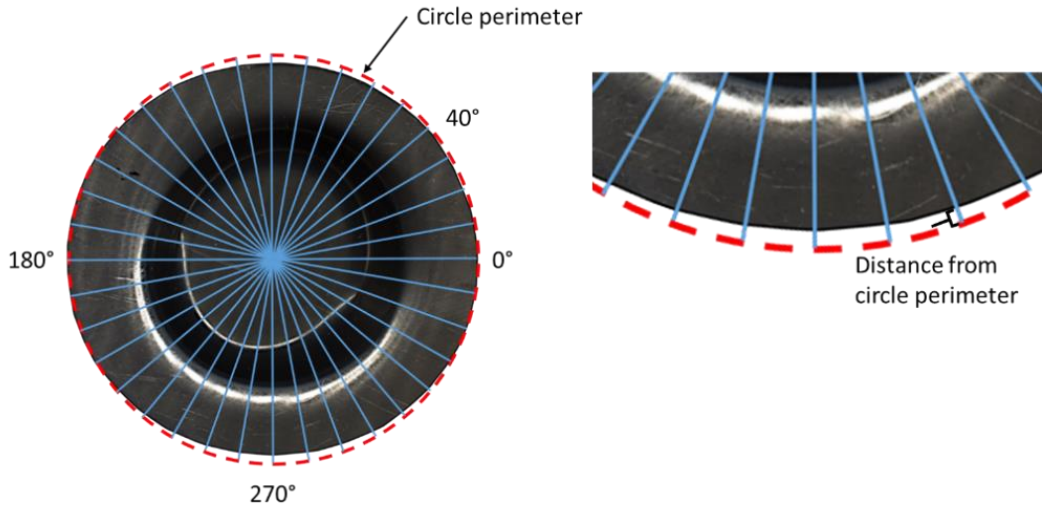

Figure 18. A schematic of how the earring profile was measured on the drawn cups. The cup shown in this image was drawn using a 203.2 mm AA7075 blank cup drawn to a depth of 55 mm.

The FE model used the modified Voce temperature- and strain rate-dependent stress-strain curves shown in Figure 15 and Figure 16. The Barlat Yld2000 yield surface coefficients from Table 16 in Appendix B were used for each of the two respective alloys. To model the heat transfer between the blank and tooling, the HTC values from Table 7 (see Section 4.3, below) were input as a function of contact pressure (Section 4.3 and Appendix C discuss how the HTC values were obtained).

The measured and predicted (from both constitutive fits shown in Figure 15 and Figure 16) force-displacement curves are shown in Figure 19a for AA7075 and Figure 19b for AA7xxx. The AA7075 blanks displayed a higher force than their AA7xxx counterparts. The predicted curves matched well with the measured curves for all four cases in Figure 19. The 177.8 mm blanks experienced a lower force than the 203.2 mm blanks, as expected. The predicted force-displacement curves were noisier than the experimental curves, although they still followed the general profile of the experimental curves. The noise in the predicted curve may be due to the implementation of the user-defined material subroutine used for these simulations.

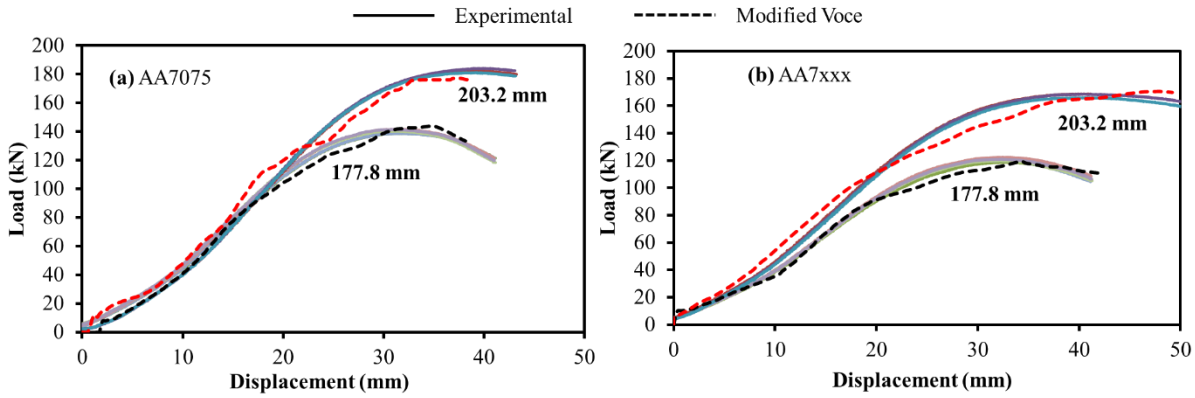

Figure 19. Measured and predicted F-D curves for (a) AA7075 and (b) AA7xxx.

The earring profiles of each of the four types of cups formed are shown in Figure 20, along with the standard deviations. The profiles predicted by the FE simulations are also shown. The experimental earring profiles were found to be symmetric, to within the measurement standard deviations, which were 0.3 mm or less. The model under-predicted the extent of earring in the transverse direction of the AA7xxx cups. The under-prediction is likely a result of the anisotropy in this alloy, wherein the r-values were reported to be as high as 1.8 in Table 4. To better capture the earring in the TD of AA7xxx, a more advanced yield surface formulation, such as Yld2004 [84], is needed.

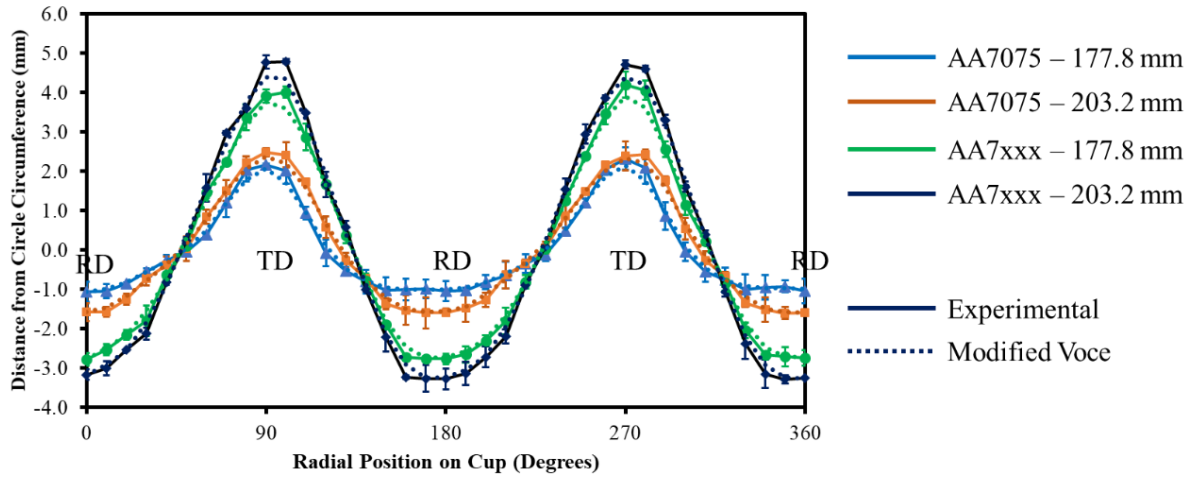

Figure 20. Earring profiles of the deep drawn cups. The rolling (RD) and transverse (TD) directions are indicated.

4.3. Heat Transfer Coefficient (HTC)

A crucial aspect in accurately modelling the DQ process is the HTC between the blank and the tooling. Appendix C contains an in-depth discussion of the HTC calculation, while following subsections provide an overview. It should be noted that Appendix C contains HTC values for several alloys and not just the two 7000-series alloys that were the focus of the current thesis.

4.3.1. Experimental Setup

The HTC experiments were conducted using 125 mm x 125 mm blanks with a milled cut-out measuring 19.4 mm in width and 100 mm in length (as shown in Figure 7b). A type k thermocouple was attached to the inside edge of the cut-out, using high temperature tape. The thermocouple was connected to an Omega OMB-DAQ-55 data acquisition system. A second thermocouple was attached to the surface of the die, as shown in Figure 21.

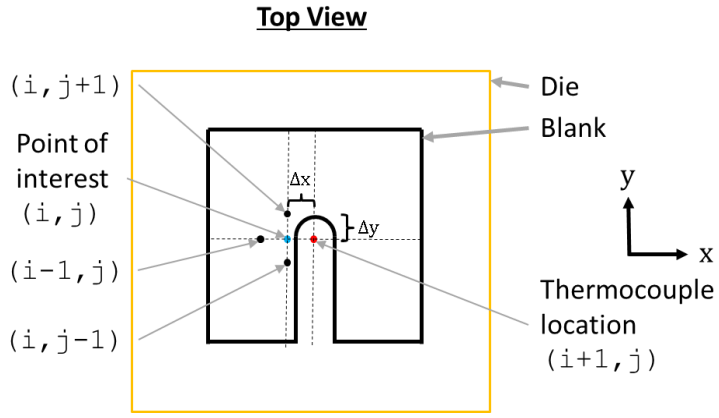

Figure 21. Thermocouple location in the die and points of interest for Eq. 6**.**

The experimental procedure consisted of the following steps:

1. The AA7075 or AA7xxx blanks were placed into a convection furnace heated to 470 °C. The thermocouple was attached to the blank prior to placement in the furnace.

2. Once the blank reached 470 °C, it was transferred from the furnace into the pair of flat dies, which are pictured in Figure 7a.
3. The blank was quenched in the dies at a desired contact pressure.

4.3.2. HTC Calculation

To determine the HTC, the following three steps were followed:

1. The experimentally obtained temperature-time curves were filtered to reduce noise.
2. The die temperature was corrected for its location.
3. The HTC was calculated using a least squares regression.

For step 1, a 5-point moving average filter was applied to the temperature-time curves obtained for the blank and the die.

For step 2, the measured die temperature needed to be corrected since the location at which the die thermocouple was placed was not in direct contact with the blank (shown in Figure 21b). The correction was done using the steady state equation for conduction:

$$\frac{\partial}{\partial x}\left(k\frac{\partial T}{\partial x}\right)+\frac{\partial}{\partial y}\left(k\frac{\partial T}{\partial y}\right)=q_{in}$$

Eq. 6

where k is thermal conductivity of the die, T is the die temperature, q_{in} is the heat flux into the die and x and y represent position. If Eq. 6 is discretized using a central difference approximation, and assuming that intervals in the *x* and *y* directions are equal ($\Delta x = \Delta y$), then

$$T_{i,j}^{n}=T_{i+1,j}^{n}+q_{in}\left(\frac{\Delta x^{2}}{k}\right)$$

Eq. 7

where the superscript n represents instance in time, the subscripts i and j represent locational coordinates (as shown in Figure 21b) on the die and Δx is the space between two points of interest. If the heat flux from the blank is equal to the heat flux into the die, Eq. 7 becomes

$$T_{i,j}^{n} = T_{i+1,j}^{n} + C_{p_{blank}} \frac{m_{blank}}{A_{blank}} \left(\frac{T_{blank}^{n+1} - T_{blank}^{n}}{\Delta t} \right) \left(\frac{\Delta x^2}{k} \right)$$

Eq. 8

where $C_{p_{blank}}$ is the specific heat capacity of the blank, m is the mass of the blank, A is the cross-sectional area of the blank that makes contact with the die surface and Δt is the time step. Using Eq. 8, the measured die temperature (*i.e.*, $T_{i+1,j}^{n}$) can be corrected to determine the die temperature at the location of contact with the blank (*i.e.*, $T_{i,j}^{n}$).

The final step, step 3, utilized the corrected die temperature. The value of the HTC was calculated using Newton's cooling law:

$$T = T_{die} + (T_o - T_{die}) e^{-\frac{hA}{mC_p} t}$$

Eq. 9

In Eq. 9, T is the measured temperature-time curve in the blank, T_o is the initial temperature of the blank. Discretizing Eq. 9 and applying a least squares regression to identify the HTC yields:

$$h = \frac{\sum \left[\ln \left(\frac{T - T_{die}}{T - T_0} \right) C_{p_{blank}} \frac{m_{blank}}{A_{blank}} \times t \right]}{\sum t^2}$$

Eq. 10

4.3.3. Results

Table 7 shows the calculated values for HTC at different contact pressures for AA7075 and AA7xxx. Figure 22 plots the HTC of unlubricated AA7075 as a function of contact pressure,

showing the strong dependence of HTC on contact pressure. For the pressures at which both alloys were tested, the HTC of AA7075 did not differ significantly from AA7xxx. Therefore, it was assumed that both alloys had the same HTC in the FE model for the deep draw simulations in Section 4.2.3.

The effect of adding different lubricants, as well as the initial blank temperature at the start of quenching, was also investigated for AA7075. The two lubricants, Fuchs ForgeEase AL278 and a Polytetrafluoroethylene (PTFE) spray, slightly lowered the HTC, but not more than 4%. Both of these lubricants were dry films (*i.e.*, they were not liquid). It is possible that wet lubricants may have a larger effect on HTC. A blank start temperature of 300 °C versus 470 °C also had negligible impact on HTC.

Table 7. Calculated HTC values and their standard deviation in parentheses (W/m^2K). Each column represents HTC at a certain contact pressure, except the column titled "NC", which denotes natural convention.

Material	**2 MPa**	**5 MPa**	**10 MPa**	**20 MPa**	**40 MPa**	**60 MPa**	**80 MPa**	**NC**
AA7075 (heated to 300 °C; dry)	355 (5)	501 (8)	620 (10)	750 (8)	1010 (19)	1800 (49)	2809 (34)	20.5
AA7075 (heated to 470 °C; dry)		498 (8)	620 (10)	750 (8)	995 (23)	1831 (39)		
AA7075 (heated to 300 °C; Fuchs ForgeEase AL278 lubricant)		481 (13)		737 (21)		1770 (67)		
AA7075 (heated to 300 °C; PTFE spray lubricant)		480 (15)		732 (21)		1783 (70)		
AA7xxx (heated to 300 °C; dry)		500 (8)		767 (16)			2772 (55)	

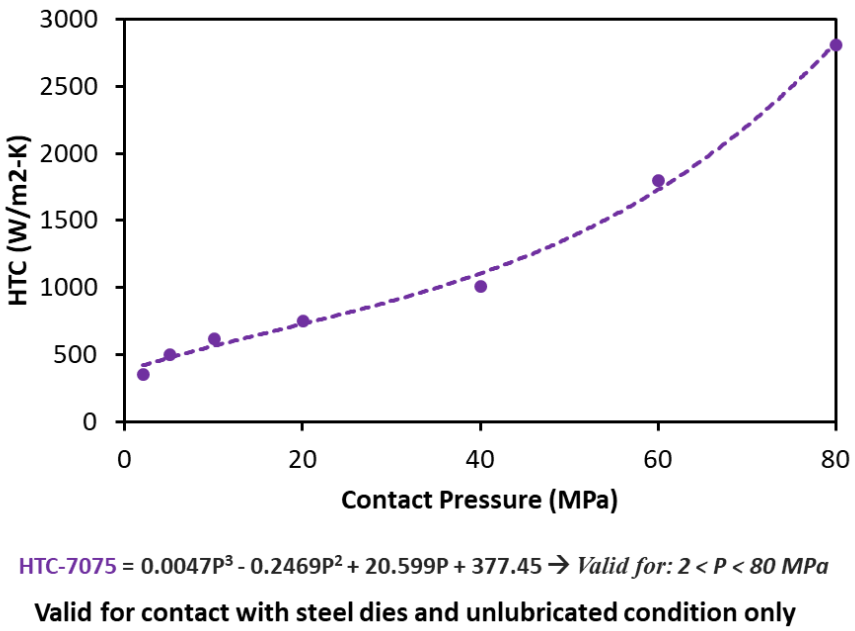

Figure 22. HTC of AA7075 with no lubricant and a start temperature of 300 °C.

4.4. Precipitate-work hardening interaction model – Post-Forming

A final requirement needed to simulate the DQ process chain (Figure 6) is to predict the final stress-strain behaviour after artificial aging following forming and die quenching. As discussed in Section 2.5 of the Literature Review, considerable past work has been done to predict the increase in yield strength during artificial aging; however, very little work has been done to predict the work hardening response beyond initial yield, particularly for the current 7000-series sheet alloys. To address this need, the current section outlines the development of a micro-mechanics based model that can predict the stress-strain response of AA7075 based on the aging treatment applied to it. Note that Appendix D provides more detail concerning this model.

4.4.1. Model Development

The work hardening model adopted in this work (referred henceforth as the precipitate-work hardening interaction model) is an amalgamation of several existing models in literature. The

governing equation of the model is due to Cheng *et al.* [73] and considers the interaction of four strengthening contributions, given by

$$\sigma = \sigma_i + \sigma_{ss} + \left(\sigma_{ppt}^n + \sigma_{dis}^n\right)^{1/n}$$

Eq. 11

where σ is the flow stress of the material, σ_i is the intrinsic strength of a pure aluminum matrix (9 MPa [79]) and σ_{ss} represents the yield strength from the solid solution. Of particular interest is the interaction of the precipitation hardening term, σ_{ppt}, and the increase in strength caused by the accumulation of dislocations (which is dependent on plastic strain), described by σ_{dis}. Cheng *et al.* [73] introduced a hardening exponent, n, to capture this interaction.

σ_{ss} can be calculated using

$$\sigma_{ss} = \sigma_{0ss}\left(1 - \alpha f_r\right)^{2/3}$$

Eq. 12

where σ_{0ss} is the yield strength of AA7075 in its supersaturated solid solution state (148 MPa, as determined from the testing discussed in Appendix A), α can be assumed to be 1 and f_r is the relative volume fraction of precipitates [75].

The term σ_{ppt}, represents the contribution of precipitates to the yield strength of the aged alloy. The strong obstacle assumption for precipitates, as defined by Esmaeili *et al.* [68], results in the following formulation for σ_{ppt}:

$$\sigma_{ppt} = C_1 f_r^{1/2}$$

Eq. 13

where C_1 can be obtained from the yield strength of the peak-aged alloy.

For n, Fazeli *et al.* [74] proposed

$$n = 1.5 + 0.5 \tanh\left(\frac{{}^{R}/_{R_C} - 1}{\chi}\right)$$

Eq. 14

where R is the average precipitate radius after the aging treatment, R_C is the average precipitate radius at which the shearable/non-shearable transition occurs and χ is a calibration parameter that governs the abruptness of the shearable/non-shearable transition.

σ_{ppt} was determined from kinetic parameters for precipitation hardening reported by Abolhasani *et al.* [85]. Details are in Sections 2 and 4 of Appendix D.

The final term in Eq. 11, σ_{dis}, can be determined by taking a linear derivative with respect to the work hardening rate (WHR) of the material:

$$\Delta\sigma_{dis} = \theta\Delta\varepsilon_p$$

Eq. 15

θ refers to the instantaneous WHR of the material and ε_p refers to true plastic strain. θ can be calculated using

$$\theta = \theta_0\left(1 - \frac{\sigma_{dis}}{\sigma_s}\right)$$

Eq. 16

where θ_0 and σ_s are calibration parameters that need to be fit using experimental data [74]. θ_0 is related to the initial hardening rate of the material and σ_s is a scaling factor accounting for the absence of precipitates.

4.4.2. Model Parameters

Table 8 summarizes the parameters required in the precipitate-work hardening interaction model.

Table 8. Calibration and other parameters used for the stress-strain model for AA7075.

Parameter	Value	Source
σ_i from Eq. 11	9 MPa	ASM Handbook [79]
R_C from Eq. 14	4.6 nm	Danh *et al.* [86]
χ in Eq. 14	0.2	Fazeli *et al.* [74]
σ_{0ss} in Eq. 12	148 Mpa	Omer *et al.* [76]
α in Eq. 12	1	Assumed, based on Sepehrband and Esmaeili [75]
C_1 in Eq. 13	488 MPa	Abolhasani *et al.* [85]
θ_0 in Eq. 16	3386 MPa	Calibrated
σ_s in Eq. 16	280 MPa	Calibrated

4.4.3. Model Application

As an application of the precipitate-work hardening interaction model, the parameters in Table 8 were used to predict the stress-strain curves for several aging conditions for AA7075, which are shown in Figure 23 alongside the stress-strain curves obtained from tensile tests. The hardening response was predicted well by the model for the complete range of aging conditions considered. Figure 24 shows the predicted WHR for each of the conditions in Figure 23. As expected, greater amounts of aging (natural or artificial) reduced the WHR. For example, in the plot on the left in Figure 24, the T6 temper, which is peak-aged for which $f_r = 1$, experienced the lowest hardening rate. The T6 temper was followed by the 7-day naturally aged (NA) specimens, then the 2-day naturally aged and finally, the 1-day naturally aged (essentially W temper) specimens.

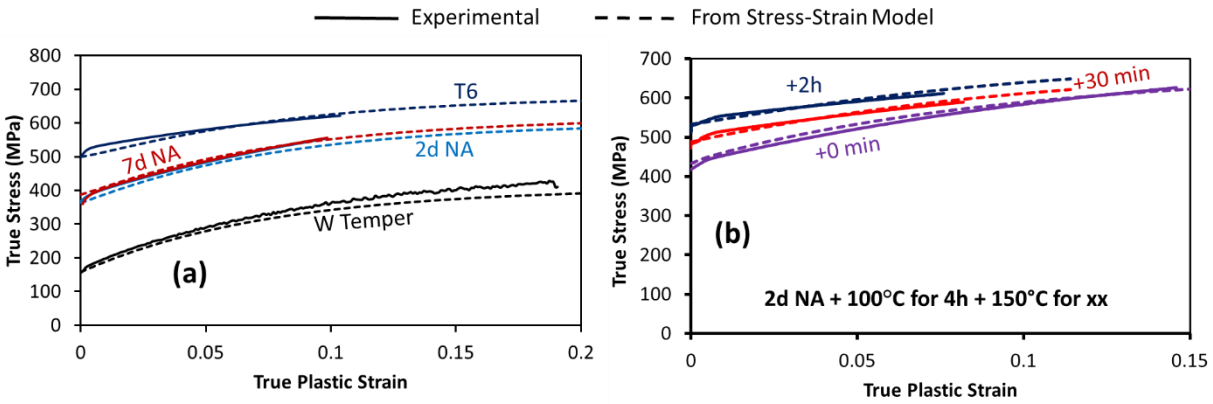

Figure 23. Stress-strain curves predicted using the stress-strain model.

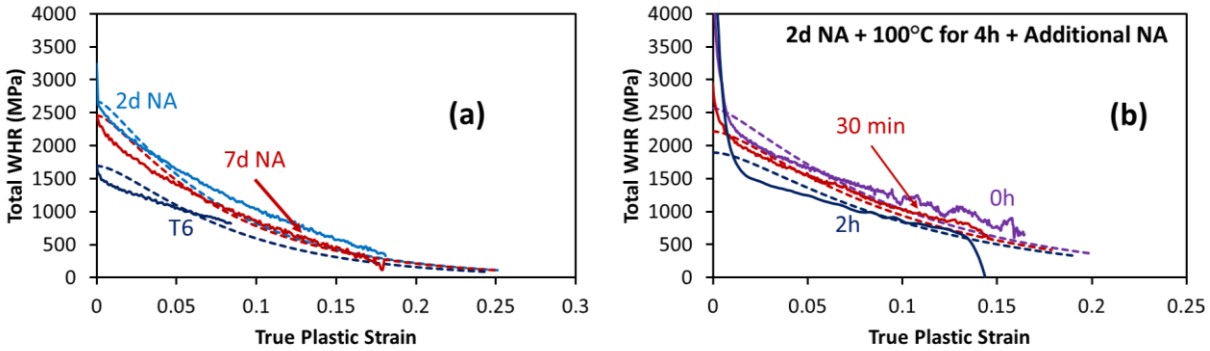

Figure 24. WHR curves predicted using the WHR model.

5. Summary and Conclusions

5.1. Summary

The current work has served to advance our understanding of and ability to model key aspects of the DQ process chain (Figure 6). The material and process data and models can enable design of more optimal DQ processes and more accurate prediction of DQ component properties. Specifically, the following original contributions are made:

1. The identification of the necessary parameters needed to die quench AA7075 and AA7xxx;
2. The discovery of aging treatments that incorporate the paint bake cycle after die quenching in order to achieve properties similar to a T6 and/or T76 temper;
3. The constitutive characterization, through the novel area reduction method, of the two alloys and their response when subjected to the temperature-time cycle of a DQ operation;
4. The technique developed to calculate HTC, as well as verification of the validity of the assumptions in that technique; and,
5. The amalgamation of several models in the literature into the precipitate-work hardening interaction model that can predict the stress-strain response of AA7075 based on the applied aging treatment (up to peak aging).

The studies of the die quenching process parameters have identified process windows required to successfully die quench the two 7000-series alloys, AA7075 and the developmental AA7xxx. The parameters provide insight to the sensitivities of the two alloys to transfer time and quench rate during die quenching, and identify the potential use and limitations of these alloys within the

DQ process. In this regard, the lower quench sensitivity of the developmental AA7xxx alloy is very attractive, providing a much larger process window for furnace-to-die transfer and tolerating lower in-die quench rates relative to AA7075.

Aging treatments were also identified that could replicate the mechanical properties of a T6 temper for AA7075 and a T6 and a T76 temper for AA7xxx, when PBC was also included as the last step of the aging schedules. Including the PBC into the aging cycle is an important aspect for automotive applications and offers the potential for increasing the efficiency of production through considerably reduced aging times prior to PBC and thus thermal energy consumption.

The constitutive model developed for die quenching was shown, through deep draw experiments, to accurately predict the load-displacement responses and earring profiles. The accuracy of the predicted earring profiles indicates that the calibrated yield surface captured the anisotropic properties of both alloys well. Likewise, the accuracy in the load-displacement predictions indicates that the stress-strain curves derived from the area reduction method capture the work hardening behaviour of both alloys during die quenching. This constitutive model can, therefore, be used to model a die quenching process.

To model the properties of the part after die quenching, and after aging, the precipitate-work hardening interaction model was developed. The model accounted for individual contributions to strength caused by precipitates and dislocations, and their interaction as deformation level increases. The model was calibrated for AA7075 and is applicable to under-aged and peak-aged conditions of this alloy, as shown in the model application in Section 4.4.3. The precipitate-dislocation model can be used in conjunction with the constitutive model for die quenching, so

that the entire process chain can be modelled from its solutionizing step to its in-service step (as pictured in Figure 6)

5.2. Conclusions

Based on the results of this thesis, the following conclusions can be drawn:

- The developmental alloy AA7xxx exhibited lower quench sensitivity and a higher tolerance to transfer time than AA7075, making AA7xxx a more desirable alloy for die quenching. There is, however, potential to die quench AA7075 as well, albeit with a tighter process window.
- The paint bake cycle can be leveraged to achieve mechanical properties close a T6 temper for AA7075 and AA7xxx and a T76 temper for AA7xxx.
- Tensile testing of both alloys in a solutionized condition revealed a work hardening rate (WHR) close to zero at 470 °C and a positive WHR for lower temperatures. Lower temperatures generally resulted in a higher WHR.
- The temperature- and strain rate-dependent generalized Voce model, calibrated in this work, accurately captured the measured true stress-strain curves for solutionized AA7075 and AA7xxx.
- The anisotropy of solutionized AA7075 and AA7xxx did not change significantly with temperature. For this reason, only one set of yield surface coefficients is required for each alloy.
- The measured heat transfer coefficient (HTC) for the AA7075 and AA7xxx alloys, in contact with a pair of steel dies, increased with contact pressure. The presence of lubricant on the

blanks slightly lowered the HTC, but no more than 4%. The initial temperature at the start of quenching (300 °C versus 470 °C) had a negligible effect on HTC.

- The constitutive and HTC models, when applied to simulation the die quench deep draw operations, accurately predicted the load-displacement and earring profiles.
- The precipitate-work hardening interaction model developed in this work can accurately predict the flow stress response of AA7075 subject to under-aged or peak-aged heat treatments, based on the individual strength mechanisms caused by precipitation hardening, dislocation strength and the relative volume fraction of precipitates present.

6. Future Work

Three areas are identified as being important for future research concerning the die quenching forming process. First, the effect of deformation during the DQ process on the subsequent age hardenability was not considered. Similarly, the precipitate-work hardening interaction model (from Section 4.4) did not directly include deformation effects during the quenching stage of the DQ process. Deformation during quenching can increase dislocation density, which can lead to a lower potential for age hardenability post-quenching.

Second, the precipitate-dislocation strength model is not applicable for overaged tempers since it did not consider precipitate coarsening. Overaged tempers are expected to see application in structural automotive parts, partially because 7000-series alloys tend to have better corrosion resistance in overaged than underaged tempers [61].

Finally, while this thesis did account for strain rate dependency in the constitutive model for die quenching, rate effects were not considered in the precipitate-work hardening interaction model. Some work addressing room temperature strain rate sensitivity of these alloys in the T6 and T76 tempers has been performed by Rahmaan *et al.* [41], however, future work should introduce rate effects in the precipitate-work hardening interaction model.

References

[1] Tajally M, Emadoddin E. Mechanical and anisotropic behaviors of 7075 aluminum alloy sheets. Mater Des 2011;32:1594–9. doi:10.1016/j.matdes.2010.09.001.

[2] Sotirov N, Simon P, Chimani C, Uffelmann D, Melzer C. Warm Deep Drawability of Peak-Aged 7075 Aluminium Sheet Alloy. Key Eng Mater 2012;504–506:955–60. doi:10.4028/www.scientific.net/KEM.504-506.955.

[3] Lin YC, Li LT, Xia YC, Jiang YQ. Hot deformation and processing map of a typical Al-Zn-Mg-Cu alloy. J Alloys Compd 2013;550:438–45. doi:10.1016/j.jallcom.2012.10.114.

[4] Rajamuthamilselvan M, Ramanathan S. Hot deformation behaviour of 7075 alloy. J Alloys Compd 2011;509:948–52. doi:10.1016/j.jallcom.2010.09.139.

[5] Rokni MR, Zarei-Hanzaki A, Roostaei AA, Abedi HR. An investigation into the hot deformation characteristics of 7075 aluminum alloy. Mater Des 2011;32:2339–44. doi:10.1016/j.matdes.2010.12.047.

[6] Deschamps A, Bréchet Y. Influence of quench and heating rates on the ageing response of an Al–Zn–Mg–(Zr) alloy. Mater Sci Eng A 1998;251:200–7. doi:10.1016/S0921-5093(98)00615-7.

[7] Lumley RN, Polmear IJ, Morton a. J. Development of mechanical properties during secondary aging in aluminium alloys. Mater Sci Technol 2005;21:1025–32. doi:10.1179/174328405X51875.

[8] Erdoğan M, Erçetin A, Güneş İ. Investigation of Mechanical Properties of Natural Aged Aa 7075 Aluminum Alloy 2014:15–7.

[9] Chen S, Chen K, Peng G, Jia L, Dong P. Effect of heat treatment on hot deformation behavior and microstructure evolution of 7085 aluminum alloy. Mater Des 2012;25:93–8.

[10] Clark R, Coughran B, Traina I, Hernandez A, Scheck T, Etuk C, et al. On the correlation of mechanical and physical properties of 7075-T6 Al alloy. Eng Fail Anal 2005;12:520–6. doi:10.1016/j.engfailanal.2004.09.005.

[11] Mahathaninwong N, Plookphol T, Wannasin J, Wisutmethangoon S. T6 heat treatment of rheocasting 7075 Al alloy. Mater Sci Eng A 2012;532:91–9. doi:10.1016/j.msea.2011.10.068.

[12] Robinson JS, Tanner DA, Truman CE, Paradowska AM, Wimpory RC. The influence of quench sensitivity on residual stresses in the aluminium alloys 7010 and 7075. Mater Charact 2012;65:73–85. doi:10.1016/j.matchar.2012.01.005.

[13] Caron EJFR, Daun KJ, Wells M a. Experimental heat transfer coefficient measurements during hot forming die quenching of boron steel at high temperatures. Int J Heat Mass Transf 2014;71:396–404. doi:10.1016/j.ijheatmasstransfer.2013.12.039.

[14] Deschamps a, Esmaeili S, Poole WJ, Militzer M. Strain hardening rate in relation to microstructure in precipitation hardening materials. J Phys Iv 2000;10:151–6.

doi:10.1051/jp4:2000626.

[15] Ozturk F, Sisman A, Toros S, Kilic S, Picu RC. Influence of aging treatment on mechanical properties of 6061 aluminum alloy. Mater Des 2010;31:972–5. doi:10.1016/j.matdes.2009.08.017.

[16] Li JF, Peng ZW, Li CX, Jia ZQ, Chen WJ, Zheng ZQ. Mechanical properties, corrosion behaviors and microstructures of 7075 aluminium alloy with various aging treatments. Trans Nonferrous Met Soc China (English Ed 2008;18:755–62. doi:10.1016/S1003-6326(08)60130-2.

[17] Viana F, Pinto a. MP, Santos HMC, Lopes a. B. Retrogression and re-ageing of 7075 aluminium alloy: microstructural characterization. J Mater Process Technol 1999;92–93:54–9. doi:10.1016/S0924-0136(99)00219-8.

[18] Koç M, Culp J, Altan T. Prediction of residual stresses in quenched aluminum blocks and their reduction through cold working processes. J Mater Process Technol 2006;174:342–54. doi:10.1016/j.jmatprotec.2006.02.007.

[19] Dolan GP, Robinson JS. Residual stress reduction in 7175-T73, 6061-T6 and 2017A-T4 aluminium alloys using quench factor analysis. J Mater Process Technol 2004;153–154:346–51. doi:10.1016/j.jmatprotec.2004.04.065.

[20] Liu S, Zhong Q, Zhang Y, Liu W, Zhang X, Deng Y. Investigation of quench sensitivity of high strength Al-Zn-Mg-Cu alloys by time-temperature-properties diagrams. Mater Des 2010;31:3116–20. doi:10.1016/j.matdes.2009.12.038.

[21] Liu S dan, Zhang X ming, Chen M an, You J hai, Zhang X yan. Effect of Zr content on quench sensitivity of AlZnMgCu alloys. Trans Nonferrous Met Soc China (English Ed 2007;17:787–92. doi:10.1016/S1003-6326(07)60175-7.

[22] Liu SD, Zhang XM, Chen MA, You JH. Influence of aging on quench sensitivity effect of 7055 aluminum alloy. Mater Charact 2008;59:53–60. doi:10.1016/j.matchar.2006.10.019.

[23] Lim ST, Yun SJ, Nam SW. Improved quench sensitivity in modified aluminum alloy 7175 for thick forging applications. Mater Sci Eng A 2004;371:82–90. doi:10.1016/S0921-5093(03)00653-1.

[24] Cavazos JL, Colás R. Quench sensitivity of a heat treatable aluminum alloy. Mater Sci Eng A 2003;363:171–8. doi:10.1016/S0921-5093(03)00616-6.

[25] You J-H, Liu S-D, Zhang X-M, Zhang X-Y. Influence of quench transfer time on microstructure and mechanical properties of 7055 aluminum alloy. J Cent South Univ Technol 2008;15:153–8. doi:10.1007/s11771-008-0030-y.

[26] Chobaut N, Carron D, Arsène S, Schloth P, Drezet JM. Quench induced residual stress prediction in heat treatable 7xxx aluminium alloy thick plates using Gleeble interrupted quench tests. J Mater Process Technol 2015;222:373–80. doi:10.1016/j.jmatprotec.2015.03.029.

[27] Liang ZQ, Zhang DT, Qiu C, Zhang W, Li YY. Quench Sensitivity and its Effect on the Microstructure and Mechanical Properties of an Al-Zn-Mg-Cu Aluminum Alloy. Adv Mater Res 2010;89–91:347–52.

[28] Vander Voort GF. Atlas of time-temperature diagrams for nonferrous alloys. United States: ASM International; 1991.

[29] Staley JT, Tiryakioglu M. The use of TTP curves and quench factor analysis for property prediction in aluminum alloys. Adv Metall Alum Alloy Proc from Mater Solut Conf James T Staley Honor Symp Alum Alloy Indianapolis, IN, United States, Nov 5-8, 2001 2001:6–15.

[30] Lee W-S, Sue W-C, Lin C-F, Wu C-J. The strain rate and temperature dependence of the dynamic impact properties of 7075 aluminum alloy. J Mater Process Technol 2000;100:116–22. doi:10.1016/S0924-0136(99)00465-3.

[31] Chen S, Chen K, Peng G, Chen X, Ceng Q. Effect of heat treatment on hot deformation behavior and microstructure evolution of 7085 aluminum alloy. J Alloys Compd 2012;537:338–45. doi:10.1016/j.jallcom.2012.05.052.

[32] Wang N, Ilinich A, Chen M, Luckey G, D'Amours G. A Comparison Study on Forming Limit Prediction Methods for Hot Stamping of 7075 Aluminum Sheet. Int J Mech Sci 2018;151:444–60. doi:10.1016/J.IJMECSCI.2018.12.002.

[33] Rahmaan T, Butcher C, Worswick MJ. Constitutive response of AA7075-T6 aluminum alloy sheet in tensile and shear loading. SEM XIII Int'l. Congr., Orlando, FL, USA: 2016.

[34] Smerd R, Winkler S, Salisbury C, Worswick M, Lloyd D, Finn M. High strain rate tensile testing of automotive aluminum alloy sheet. Int J Impact Eng 2005;32:541–60. doi:10.1016/j.ijimpeng.2005.04.013.

[35] Chen Y, Clausen AH, Hopperstad OS, Langseth M. Stress-strain behaviour of aluminium alloys at a wide range of strain rates. Int J Solids Struct 2009;46:3825–35. doi:10.1016/j.ijsolstr.2009.07.013.

[36] Miller W., Zhuang L, Bottema J, Wittebrood a. ., De Smet P, Haszler a, et al. Recent development in aluminium alloys for the automotive industry. Mater Sci Eng A 2000;280:37–49. doi:10.1016/S0921-5093(99)00653-X.

[37] Oosterkamp LD, Ivankovic A, Venizelos G. High strain rate properties of selected aluminium alloys. Mater Sci Eng A 2000;278:225–35. doi:10.1016/S0921-5093(99)00570-5.

[38] Li D, Ghosh A. Tensile deformation behavior of aluminum alloys at warm forming temperatures. Mater Sci Eng A 2003;352:279–86. doi:10.1016/S0921-5093(02)00915-2.

[39] Lin YC, Dong WY, Zhou M, Wen DX, Chen DD. A unified constitutive model based on dislocation density for an Al-Zn-Mg-Cu alloy at time-variant hot deformation conditions. Mater Sci Eng A 2018;718:165–72. doi:10.1016/j.msea.2018.01.109.

[40] Azarbarmas M, Aghaie-Khafri M, Cabrera JM, Calvo J. Dynamic recrystallization mechanisms and twining evolution during hot deformation of Inconel 718. Mater Sci Eng A 2016;678:137–52. doi:10.1016/j.msea.2016.09.100.

[41] Rahmaan T, Bardelcik A, Imbert J, Butcher C, Worswick MJ. Effect of strain rate on flow stress and anisotropy of DP600, TRIP780, and AA5182-O sheet metal alloys. Int J Impact Eng 2016;88:72–90. doi:10.1016/j.ijimpeng.2015.09.006.

[42] Ozturk F, Esener E, Toros S, Picu CR. Effects of aging parameters on formability of 6061-O alloy. Mater Des 2010;31:4847–52. doi:10.1016/j.matdes.2010.05.050.

[43] Ghosh M, Miroux a., Werkhoven RJ, Bolt PJ, Kestens L a I. Warm deep-drawing and post drawing analysis of two Al-Mg-Si alloys. J Mater Process Technol 2014;214:756–66. doi:10.1016/j.jmatprotec.2013.10.020.

[44] Abedrabbo N, Pourboghrat F, Carsley J. Forming of AA5182-O and AA5754-O at elevated temperatures using coupled thermo-mechanical finite element models. Int J Plast 2007;23:841–75. doi:10.1016/j.ijplas.2006.10.005.

[45] Leacock AG, Howe C, Brown D, Lademo OG, Deering A. Evolution of mechanical properties in a 7075 Al-alloy subject to natural ageing. Mater Des 2013;49:160–7. doi:10.1016/j.matdes.2013.02.023.

[46] Karabin ME, Barlat F, Schultz RW. Numerical and experimental study of the cold expansion process in 7085 plate using a modified split sleeve. J Mater Process Technol 2007;189:45–57. doi:10.1016/j.jmatprotec.2007.01.008.

[47] Deng Y, Yin Z, Huang J. Hot deformation behavior and microstructural evolution of homogenized 7050 aluminum alloy during compression at elevated temperature. Mater Sci Eng A 2011;528:1780–6. doi:10.1016/j.msea.2010.11.016.

[48] Toros S, Ozturk F, Kacar I. Review of warm forming of aluminum–magnesium alloys. J Mater Process Technol 2008;207:1–12. doi:10.1016/j.jmatprotec.2008.03.057.

[49] Hill R. Constitutive modelling of orthotropic plasticity in sheet metals. J Mech Phys Solids 1990;38:405–17. doi:10.1016/0022-5096(90)90006-P.

[50] Barlat F, Lian K. Plastic behavior and stretchability of sheet metals. Part I: A yield function for orthotropic sheets under plane stress conditions. Int J Plast 1989;5:51–66. doi:10.1016/0749-6419(89)90019-3.

[51] Barlat F, Brem JC, Yoon JW, Chung K, Dick RE, Lege DJ, et al. Plane stress yield function for aluminum alloy sheets - Part 1: Theory. Int J Plast 2003;19:1297–319. doi:10.1016/S0749-6419(02)00019-0.

[52] Rahmaan T, Abedini A, Zhou P, Butcher C, Worswick MJ. Anisotropic plasticity characterization of 6000- and 7000-series aluminum sheet alloys at various strain rates. Int J Impact Eng 2019:103390. doi:10.1016/j.ijimpeng.2019.103390.

[53] Khan AS, Baig M. Anisotropic responses, constitutive modeling and the effects of strain-rate and temperature on the formability of an aluminum alloy. Int J Plast 2011;27:522–38. doi:10.1016/j.ijplas.2010.08.001.

[54] Abedrabbo N, Pourboghrat F, Carsley J. Forming of aluminum alloys at elevated temperatures - Part 1: Material characterization. Int J Plast 2006;22:314–41. doi:10.1016/j.ijplas.2005.03.005.

[55] Malinowski Z, Lenard JG, Davies ME. A study of the heat-transfer coefficient as a function of temperature and pressure. J Mater Process Tech 1994;41:125–42. doi:10.1016/0924-0136(94)90057-4.

[56] Tanner D a., Robinson JS. Residual stress prediction and determination in 7010 aluminum alloy forgings. Exp Mech 2000;40:75–82. doi:10.1007/BF02327551.

[57] Merklein M, Lechler J, Stoehr T. Investigations on the thermal behavior of ultra high strength boron manganese steels within hot stamping. Int J Mater Form 2009;2:259–62. doi:10.1007/s12289-009-0505-x.

[58] Caron E, Daun KJ, Wells MA. Experimental characterization of heat transfer coefficients during hot forming die quenching of boron steel. Metall Mater Trans B Process Metall Mater Process Sci 2013;44:332–43. doi:10.1007/s11663-012-9772-x.

[59] Liu X, Ji K, Fakir O El, Fang H, Gharbi MM, Wang LL. Determination of the interfacial heat transfer coefficient for a hot aluminium stamping process. J Mater Process Technol 2017;247:158–70. doi:10.1016/j.jmatprotec.2017.04.005.

[60] Starink MJ, Wang SC. A model for the yield strength of overaged Al-Zn-Mg-Cu alloys. Acta Mater 2003;51:5131–50. doi:10.1016/S1359-6454(03)00363-X.

[61] Sevim I, Sahin S, Cuz H, Cevik E, Hayat F, Karali M. EFFECT OF AGING TREATMENT ON SURFACE ROUGHNESS, MECHANICAL PROPERTIES, AND FRACTURE BEHAVIOR OF 6XXX AND 7XXX ALUMINUM ALLOYS. Strength Mater 2014;46:190–7.

[62] Jabra J, Romios M, Lai J, Lee E, Setiawan M, Lee EW, et al. The Effect of Thermal Exposure on the Mechanical Properties of 2099-T6 Die Forgings, 2099-T83 Extrusions, 7075-T7651 Plate, 7085-T7452 Die Forgings, 7085-T7651 Plate, and 2397-T87 Plate Aluminum Alloys. J Mater Eng Perform 2006;15:601–7. doi:10.1361/105994906X136142.

[63] Deschamps A, Brechet Y. INFLUENCE OF PREDEFORMATION AND AGEING OF AN Al-Zn-Mg ALLOY-II. MODELING OF PRECIPITATION KINETICS AND YIELD STRESS. Acta Mater 1999;47:293–305. doi:S1359-6454(98)00296-1.

[64] Wagner R, Kampmann R. Materials Science and Technology, a Comprehensive Treatment. Weinheim. Germany: VCH; 1991.

[65] Poole W, SHercliff H, Castillo T. Process model for two step age hardening of 7475 aluminium alloy. Mater Sci Technol 1997;13:897–904. doi:10.1179/mst.1997.13.11.897.

[66] Shercliff HR, Ashby MF. A process model for age hardening of aluminium alloys-II. Applications of the model. Acta Metall Mater 1990;38:1803–12. doi:10.1016/0956-7151(90)90292-O.

[67] Esmaeili S, Cheng LM, Deschamps A, Lloyd DJ, Poole WJ. The deformation behaviour of AA6111 as a function of temperature and precipitation state. Mater Sci Eng A 2001;319–321:461–5. doi:10.1016/S0921-5093(01)01113-3.

[68] Esmaeili S, Lloyd DJ, Poole WJ. A yield strength model for the Al-Mg-Si-Cu alloy AA6111. Acta Mater 2003;51:2243–57. doi:10.1016/S1359-6454(03)00028-4.

[69] Esmaeili S, Lloyd D. Modeling of precipitation hardening in pre-aged AlMgSi(Cu) alloys. Acta Mater 2005;53:5257–71. doi:10.1016/j.actamat.2005.08.006.

[70] Esmaeili S, Lloyd DJ, Poole WJ. Modeling of precipitation hardening for the naturally aged Al-Mg-Si-Cu alloy AA6111. Acta Mater 2003;51:3467–81. doi:10.1016/S1359-6454(03)00167-8.

[71] Fribourg G, Brechet Y, Deschamps A, Simar A. Microstructure-based modelling of isotropic and kinematic strain hardening in a precipitation-hardened aluminium alloy. Acta Mater 2011;59:3621–35. doi:10.1016/j.actamat.2011.02.035.

[72] Deschamps A, Fribourg G, Brechet Y, Chemin JL, Hutchinson CR. In situ evaluation of dynamic precipitation during plastic straining of an Al-Zn-Mg-Cu alloy. Acta Mater 2012;60:1905–16. doi:10.1016/j.actamat.2012.01.002.

[73] Cheng LM, Poole WJ, Embury JD, Lloyd DJ. The influence of precipitation on the work-hardening behavior of the aluminum alloys AA6111 and AA7030. Metall Mater Trans A 2003;34:2473–81. doi:10.1007/s11661-003-0007-2.

[74] Fazeli F, Poole WJ, Sinclair CW. Modeling the effect of Al3Sc precipitates on the yield stress and work hardening of an Al-Mg-Sc alloy. Acta Mater 2008;56:1909–18. doi:10.1016/j.actamat.2007.12.039.

[75] Sepehrband P, Esmaeili S. Application of recently developed approaches to microstructural characterization and yield strength modeling of aluminum alloy AA7030. Mater Sci Eng A 2008;487:309–15. doi:10.1016/j.msea.2007.10.067.

[76] Omer K, Abolhasani A, Kim S, Nikdejad T, Butcher C, Wells M, et al. Process parameters for hot stamping of AA7075 and D-7xxx to achieve high performance aged products. J Mater Process Technol 2018;257:170–9. doi:10.1016/j.jmatprotec.2018.02.039.

[77] Yoon JW, Barlat F, Dick RE, Chung K, Kang TJ. Plane stress yield function for aluminum alloy sheets - Part II: FE formulation and its implementation. Int J Plast 2004;20:495–522. doi:10.1016/S0749-6419(03)00099-8.

[78] Dumont D, Deschamps a., Bréchet Y, Sigli C, Ehrström JC. Characterisation of precipitation microstructures in aluminium alloys 7040 and 7050 and their relationship to mechanical behaviour. Mater Sci Technol 2004;20:567–76. doi:10.1179/026708304225016662.

[79] ASM International. Asm Handbook: Properties and Selection : Irons, Steels, and High Performance Alloys. 10th ed. Materials Park, OH: ASM International; 1990.

[80] U.S. Government Printing Office. Heat Treatment of Aluminum Alloys. MI L -H- 6088G 1991.

[81] Livermore Software Technology Corporation (LSTC). Keyword User ' S Manual Volume 1. vol. I. Livermore, CA, USA: 2011.

[82] Livermore Software Technology Corporation (LSTC). Keyword User ' S Manual Volume II. vol. II. Livermore, CA, USA: 2014.

[83] Noder J. Characterization and Simulation of Warm Forming of 6xxx and 7xxx Series Aluminum Alloys by. University of Waterloo, 2017.

[84] Barlat F, Aretz H, Yoon JW, Karabin ME, Brem JC, Dick RE. Linear transfomation-based

anisotropic yield functions. Int J Plast 2005;21:1009–39. doi:10.1016/j.ijplas.2004.06.004.

[85] Abolhasani A, Wells M, Esmaeili S. No Title n.d.

[86] Danh NC, Rajan K, Wallace W. A TEM study of microstructural changes during retrogression and reaging in 7075 aluminum. Metall Trans A 1983;14:1843–50. doi:10.1007/BF02645554.

Appendix A

Omer K, Abolhasani A, Kim S, Nikdejad T, Butcher C, Wells M, Esmaeili S, Worswick M. Process parameters for hot stamping of AA7075 and D-7xxx to achieve high performance aged products. J Mater Process Technol 2018;257:170–9. doi:10.1016/j.jmatprotec.2018.02.039.

Accessible through the following link as well as the University of Waterloo's Institutional Repository (UW Space):

https://www.sciencedirect.com/science/article/pii/S0924013618300955

Appendix B

Omer K, Butcher C, Esmaeili S, Worswick M. Characterization and application of a constitutive model for two 7000-series aluminum alloys subjected to hot forming. Int J Mech Sci 2020;165. doi:https://doi.org/10.1016/j.ijmecsci.2019.105218.

Accessible through the following link as well as the University of Waterloo's Institutional Repository (UW Space):

https://www.sciencedirect.com/science/article/pii/S0020740318337597

Appendix C

Omer K, Butcher C, Worswick M. Characterization of heat transfer coefficient for non-isothermal elevated temperature forming of metal alloys. Int J Mater Form 2019. doi:10.1007/s12289-019-01478-3.

Accessible through the following link as well as the University of Waterloo's Institutional Repository (UW Space):

https://link.springer.com/article/10.1007/s12289-019-01478-3

Appendix D

Omer, K., Abolhasani, A., Esmaeili, S., Worswick, M., A Microstructure-Based Model to Predict the Stress-Strain Behaviour of AA7075 Following Various Aging Treatments. Submitted to Computation Materials Science 2019.